Optimization of Oral Insulin Drug Delivery via Inhalation

BEE 4530: Computer Aided Engineering: Applications to Biomedical Processes

Karen Chin
Nicholas Mulchan
Stephen Hong
Stephen Yoon

TABLE OF CONTENTS

1. Executive Summary …… 2

2. Introduction

2.1 Background …… 3

2.2 Design Objectives …… 4

2.3 Terms Defined …… 4

2.4 Problem Schematic …… 5

3. Results and Discussion

3.1 2D Laminar Model …… 7

3.2 2D Turbulent Model …… 12

3.3 3D Laminar Model …… 16

3.4 Accuracy Check …… 20

3.5 Sensitivity Analysis …… 22

4. Conclusion

4.1 Conclusions …… 24

4.2 Implications & Relevance …… 24

4.3 Design Recommendations …… 24

4.4 Realistic Constraints …… 25

Appendix A: Mathematical Statement of the Problem …… 26

Appendix B: Solution Strategy …… 34

Appendix C: Software Implementation …… 42

Appendix D: Additional Visuals …… 47

Appendix E: References …… 48

1. Executive Summary

Drug inhalation is quickly emerging in the field of drug delivery techniques, providing localized treatment for various types of lung disorders. To expand oral drug delivery, this project will focus on inhaled insulin therapy to provide a systemic treatment that will reduce the detrimental effects of diabetes. Previous research has shown that inhaled insulin is more efficient and preferable to patients compared to the commonly used insulin injection therapy. However, there are several problems associated with drug inhalation techniques, including the impaction of drug against the natural right angle geometry of the pharynx, which results in decreased deposition in the lungs. The goals of this project include the optimization of insulin drug particle diameter size, the optimization of particle density, and optimization of the peak inhalation rate of drug to reduce impaction against the pharynx and to maximize deposition in the lungs.

Optimization of the aerosol insulin was done using a laminar flow COMSOL model. To simplify the model, a two dimensional, cross-section of the mouth and trachea was used as the biological system to measure the effectiveness of the delivery scheme. This model was used to test particles with density values ranging from 10 g/m^3 to 800 g/m^3, as well as particles with diameters ranging from 1 μm to 17.5 μm. In addition, particles were tested with peak inhalation rates ranging from 15 L/min to 90 L/min and inhaler insertion angles ranging from -10° to 10°. Using every permutation of particle density, particle diameter, peak inhalation rate, and insertion angle we sought to find the most optimal delivery system for deposition at the bottom of the trachea. Particle deposition was further analyzed by varying inhalation rate and particle parameters in a 2D turbulent flow model and a 3D laminar flow model.

For the 2D laminar flow model, particle deposition was found to be the most sensitive to inhalation rate compared to the other experimental parameters. Results indicated that high inhalation rates (45-60 L/min), particles with low density (100-400 kg/m^3) and low diameter (1-7.5 μm) resulted in increased particle deposition, which agrees with literature. For the velocity profile we obtained, the peak normalized velocity values of 1.53 for the 15 L/min inhalation rate, 1.37 for the 30 L/min inhalation rate, and 1.27 for the 90 L/min inhalation rate agree with the values recorded in literature. For the 2D turbulent flow model, varying inhalation rate, particle density and diameter appeared to have no significant effect on particle deposition. The turbulent model displayed particle depositions that were an order of magnitude lower than those of the 2D laminar model, which we believe to be due to turbulent dispersion effects. For the 3D laminar flow model, flow velocity did not vary in the z direction, which implies that the 2D laminar model is an appropriate representation of flow velocity

Our model demonstrates the effects of changing various drug particle parameters on particle deposition. We recommend the use of particles with low density and low diameter along with high inhalation rates in order to reduce impaction in the oral cavity and increase deposition in the lungs. Since particle deposition was most sensitive to inhalation rate, when formulating oral drug treatment particles, the specific inhalation rate that is used should be carefully considered.

2. Introduction

2.1 Background

Drug delivery via inhalation became a popular choice of respiratory care in the 20th century[1]. While it has been recently been a "hot" topic in the field of drug delivery, the use of inhalers actually dates back to the 18th century[2]. The popularity and interest surrounding this therapy has been partly due to the rise of diagnosed respiratory disorders, particularly that of asthma in the United States from 2001 to 2010[3].

Another driving factor for the popularity of this treatment type included exploring noninvasive procedures to increase patient compliance. By varying treatment target, drug content, formulation and inhaler device design, researchers aim to deliver an optimal dose of drug content into systemic circulation via inhalation.

Inhaled drug therapy has the potential to deliver high doses of drug treatment without any adverse systemic side effects[3]. Because the drug travels through the respiratory system and eventually becomes absorbed into the bloodstream, it avoids the highly acidic and digestive environment of the stomach[3]. Also, drug delivery via inhalation is especially attractive because the human lung endothelium is very permeable[4]. Thus, in addition to respiratory disorders, a variety of non-respiratory disorders and diseases have been targeted by inhaled drug delivery.

Diabetes mellitus is a chronic disease characterized by high sugar levels in the blood that has been targeted by inhaled drug delivery. This disease affects 8.3% of the United States' population and is caused by insulin deficiency, resistance to insulin, or both[3]. Type I diabetes is caused by an autoimmune deficiency in insulin production and requires daily insulin injections[5]. The more common case, Type II diabetes, is caused by a lack of insulin production or insulin resistance[5]. Physicians have found that tight control of blood glucose levels through insulin therapy reduces the detrimental effects of diabetes[6]. The most common form of treatment has been insulin injection therapy, but there are a few disadvantages associated with the therapy. First, the therapy has been shown to be absorbed too slowly into the bloodstream (serum peak of insulin at 60-150 min) compared to natural insulin secretion from the pancreas[6]. Additionally, patients can experience pain from frequent use of insulin injection needles. A majority of patients inject themselves too few times a day because of the inconveniences the therapy causes[7].

Inhaled insulin is an alternative method that is safe, efficient, and well tolerated by patients. One research group demonstrated that Type II-diabetic patients receiving Exubera inhaled insulin therapy showed lower rates of hyperglycemia (.2 less events per month) compared to patients receiving insulin injection therapy[3]. The same group showed that 15% more patients receiving the inhaled insulin therapy reached the American Diabetes Association goal of antibody binding (<7%)[3]. Another group that conducted multiple three-month human efficacy studies showed that inhaled insulin is rapidly absorbed into the bloodstream (serum peak at 5-60 min)[4]. The same group showed that the inhaled insulin therapy was well tolerated, in that 92% of Type II diabetes patients requested for a one year extension of the therapy[5].

In general, while inhaled drug treatment is an attractive therapy option, there are several drawbacks associated with this type of therapy. A wide range and variation of inhaler device designs can lead to improper drug dosage, especially as improper inhaler technique is common among patients[8]. The main problem associated with inhaled drug delivery was low bioavailability for drug deposition[1]. In the early stages of the field, drug inhalation treatments

were only effectively delivery 10-15% of the nominal dose[1]. The decreased bioavailability can be attributed to inappropriate particle diameters that either result in particles becoming exhaled or unable to pass into the thoat[1]. Likewise, particle density then becomes an important factor that determines the deposition site of the particles[1].

Another determining factor for successful deposition into the lungs is inhaler velocity. If velocity is too high, particles become inertially impacted against the pharynx wall[3]. An optimal combination of these parameters will increase insulin particle deposition into the trachea, thus increasing bioavailability and effective therapeutic dosage.

2.2 Design Objectives

In this project, an accurate COMSOL computational model for insulin drug particles inhaled into the human oral cavity will be developed. Particle velocity and particle trajectories of these inhaled insulin drug particles will be analyzed. We aim to study how to minimize particle impaction against the pharynx, and thus maximize particle deposition into the trachea. Our computation model will be used to define the optimal combination of particle diameter, particle density, insertion angle and peak inhalation rate in order to maximum particle deposition.

2.3 Terms Defined

***Particle Density**:* insulin drug particle density values that account for mass and volume characteristics
Particle Diameter: insulin drug particle diameter values that describe particle size
***Inhalation Rate**:* volumetric flow rate of inhaled drug particles as they enter the oral cavity
Initial Particle Velocity: initial velocity of the drug particles as they enter the oral cavity
***Insertion Angle**:* angle at which the "inhaler" is positioned is thus the angle at which particles enter the oral cavity with respect to the horizontal axis

2.4 Problem Schematic

2.4.A 2D Model

A 2D model was used to examine the fluid flow and particle tracing of the insulin drug particles for the implementation in COMSOL. A sagittal plane through the medial line of the oral cavity was used as the basis of our 2D model (Fig 1). It was assumed that the z-axis geometry was not required as the flow effects in that axis are minimal compared to the x- and y-axes. The model provided three representative areas that the particles could travel through, the air-filled central oral cavity and the two mucus filled layers at the top and bottom of the oral cavity. The mucus boundary layer was assumed to possess a constant thickness of 0.1mm[9].

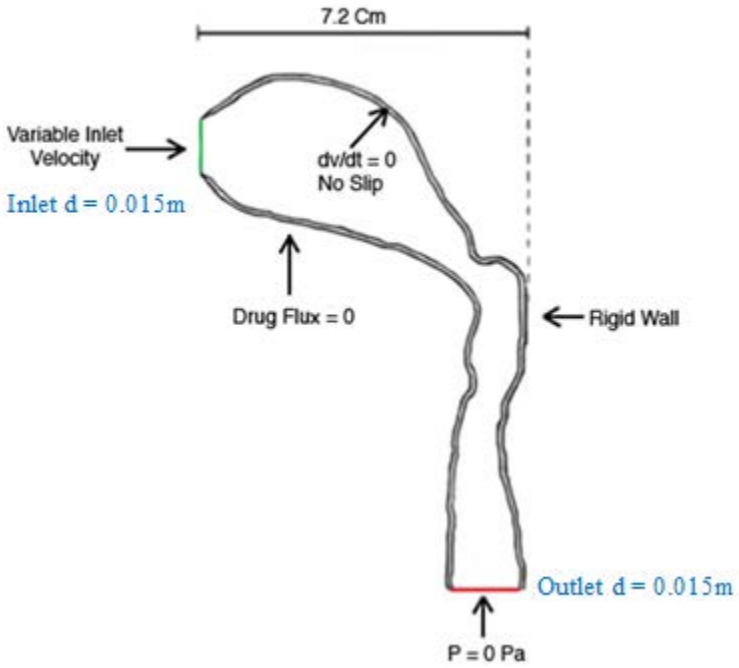

Figure 1. Schematic of the human oral cavity that will be implemented in the model (Image adapted from [5]). The 0.1mm thick mucus layer is marked in the schematic by the double-edged boundary[9]. Particles will enter the oral cavity via the inlet (diameter, d = 0.015m) labeled in green and exit at the outlet (diameter, d = 0.027m) labeled in red. Diameter values for the inlet and outlet were scaled from the scale provided[5].

The boundary layer of the oral cavity was modeled as a "stick" boundary with a probability, meaning that particles impacting any part of the oral cavity wall had a probability of sticking to the wall. For simplification purposes consistent with literature, a probability of 1 was used[10]. The model assumes uniform drug distribution at the mouth entrance prior to drug inhalation. In addition, the drug was assumed to all have uniform density and aerodynamic diameters for each treatment. The inhalation rate was implemented as a sinusoidal function to realistically model airflow during inhaled drug delivery. The particle tracing physics assumes that the main forces acting upon the particles are drag and gravitational forces. The fluid was assumed to be Newtonian and incompressible.

The laminar models assumed laminar airflow throughout the geometry. Conversely, the turbulent model assumed turbulent airflow. The turbulent model employed the same oral cavity schematic, but with the absence of the two mucus layers. The two mucus layers were not

included due to the many complications that were introduced to the model from flow eddy formation that occurred at the mucus layers.

The laminar flow model was selected due to a low Reynolds number, as the velocities of the fluid flow and fluid density were small values. Therefore, we assumed that the laminar model assumption was valid. However, we discovered that this was not true at the higher inhalation rates, and thus higher fluid velocities- this gave us motivation to test our model for turbulent flow.

2.4.B 3D Model

The same human oral cavity geometry used in the 2D laminar model was extruded 0.1m in the z-axis direction to produce a 3D oral cavity for laminar flow (Fig 2). The mucus layer boundary was not included in the 3D oral cavity walls.

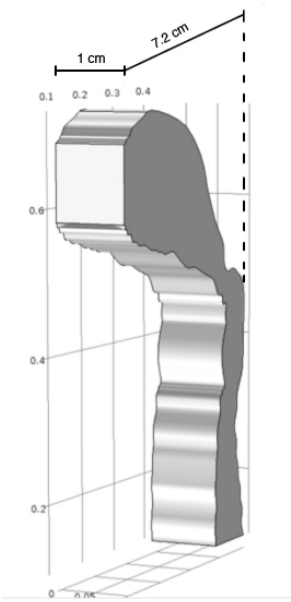

Figure 2. Schematic of the human oral cavity in 3D built by extruding the 2D schematic 0.1m in the z-direction.

3. Results and Discussion

3.1 2D Laminar Model

3.1.A Velocity Profile

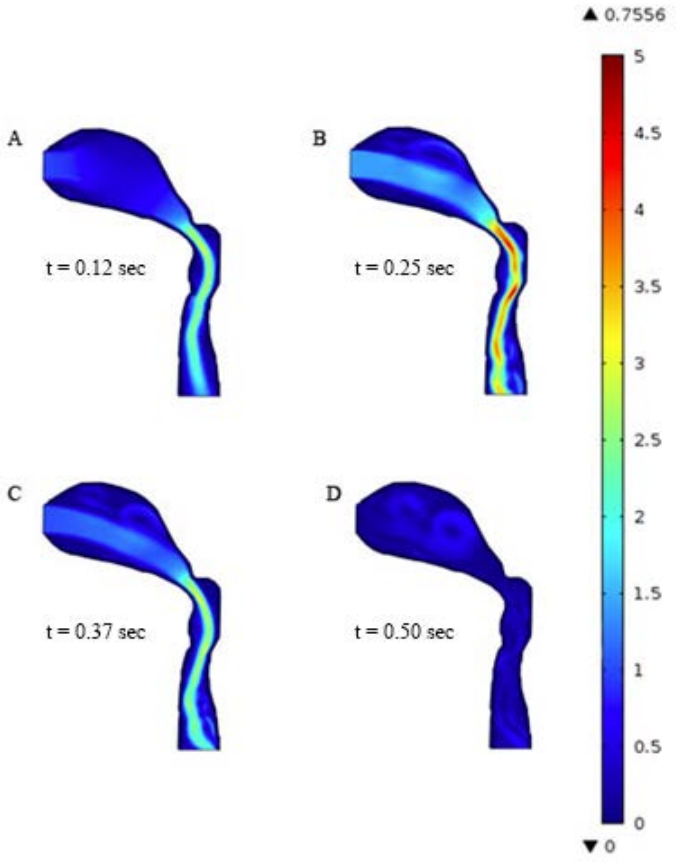

Figure 3. 2D laminar velocity profiles for time range (0: 0.01: 0.5s) at the following time points: (A) t = 0.12s (B) t = 0.25s (C) t = 0.37s (D) t = 0.5s

Velocity changed with time in the oral cavity (Fig 3). For the specified inlet inhalation rate of 30 L/min, air flow velocities increased with time to a maximum velocity of approximately 5 m/s in the trachea at t = 0.25 s (Fig 3B). The narrow diameter of the pharynx and trachea is characteristic of a “bottle-neck” region and resulted in a high concentration of increased airflow velocity due to a reduced cross-sectional area. After the peak velocity at t = 0.25 s, air flow velocities decreased due to the sine-wave function specified at the inlet velocity (Fig 3C). Similarly to the 2D model, the 3D model also displayed a “bottle-neck” region resulting in a high concentration of higher velocities in the constricted area by the pharynx. For later time points (t = 0.5s), the middle region of the oral cavity demonstrated the effect of shear stresses on velocity (Fig 3D).

3.1.B Particle Tracing

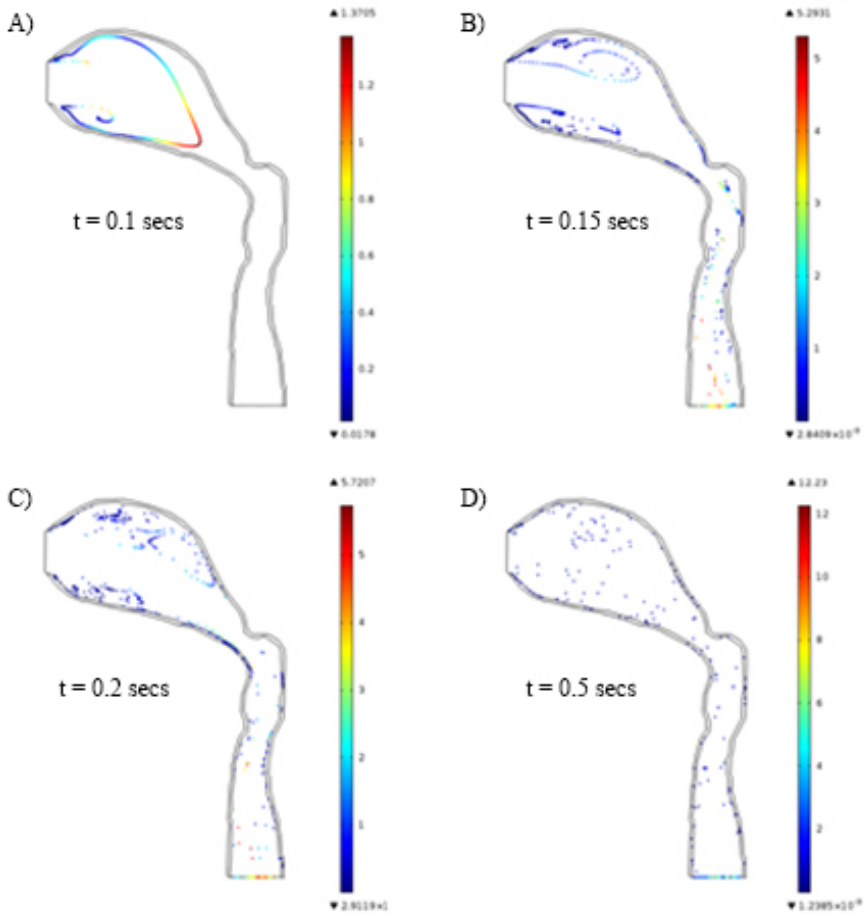

Figure 4. Particle trajectory plots in 2D laminar flow for time range (0: 0.01: 0.5s) at the time points: (A) t = 0.1s (B) t = 0.15s (C) t = 0.2s (D) t = 0.5s

Particle trajectory paths changed with time (Fig 4). For initial time points (t = 0.1 s), particles entering the oral cavity closely followed the velocity profile of the inlet airflow, forming a ring of particles that moved forward as the airflow increased from the inlet (Fig 4A). The particles with highest velocity were found at the center region of the oral cavity where the maximum airflow was observed. Conversely, particles with the lowest velocities were in close proximity to the upper and bottom mucus layers and may have experienced shear forces. A short time period later (t = 0.15s), the plots indicated that particles traveling down the trachea possessed the greatest velocity (Fig 4B). Some particle velocities decreased as they continued their pathway down the trachea, particularly those near the mucus layers (Fig 4C). This demonstrates decreased particle velocity due to the effect of particle impact against the mucus layer and stick to the pharynx wall. At later time points (t=0.5s), most of the particles have settled or are traveling at relatively low velocities (Fig 4D).

3.1.C Particle Deposition

Color intensity maps were constructed to display the results of particle fraction deposition due to varying parameters. Three sets of particle fraction deposition results are displayed (1) varying particle diameters, inhalation rates, and high particle density values (100 to 800 kg/m^3) (Fig 5), (2) varying particle diameters, inhalation rates, and low particle density values (10 to 75 kg/m^3) (Fig 6) and (3) varying insertion angle, inhalation rates, and particle density values (10 to 800 kg/m^3) (Fig 7). Overall, the highest particle fraction deposition was 8.75% for a particle diameter of 7.5µm, particle density of 200 g/cm^3, and inhalation rate of 60 L/min (Table B8).

The laminar model was most sensitive to inhalation rate compared to the other experimental parameters of particle density, and particle diameter. This was true for both the high particle densities (Fig 5) and for low density cases (Fig 6). For low and high particle densities, fraction of particle deposition ranged from approximately 0 to 0.08.

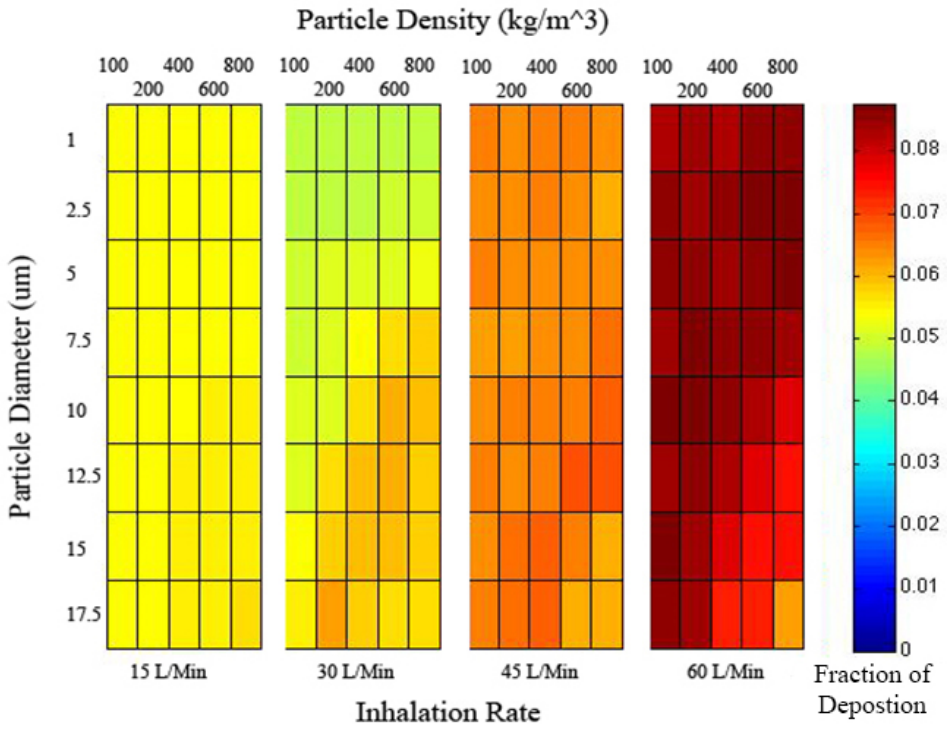

Figure 5. Color intensity map representing the 2D laminar flow deposition fraction of insulin particles as a function of particle diameter (µm), high particle density values (100-800 g/cm^3), and inhalation rate (L/min). Map was constructed based on data from Tables B9-12.

Higher flow rates (45 L/min, 60 L/min) generally have greater particle deposition as compared to the lower flow rates (15 L/min, 30 L/min) (Fig 5, 6). This was the case when inhalation rate and diameter were varied alongside the simulations for both low particle densities (Fig 6), and for high particle densities (Fig 5).

At low density values, there appears to be no significant particle deposition effect from varying particle density or diameter (Fig 6). At high density values, for lower inhalation rates, as particle diameter and density values are both increased, particle deposition increases (Fig 5). However, for higher inhalation rates, increases in particle diameter and densities resulted in decreased particle deposition (Fig 5).

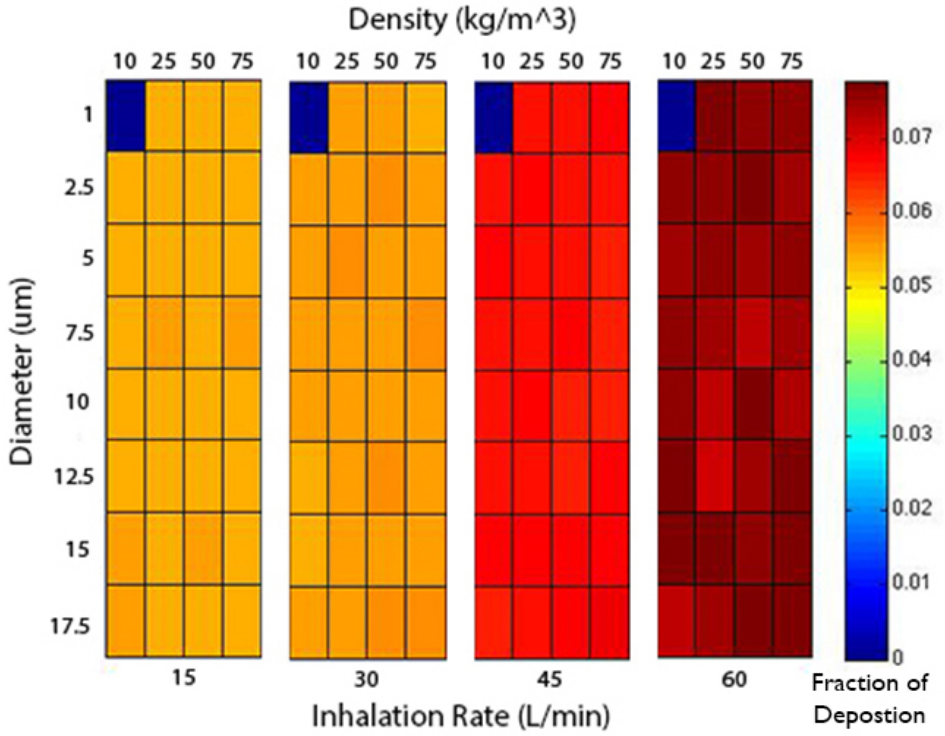

Figure 6. Color intensity map of deposition fraction of insulin particles as a function of particle diameter (μm), low particle density values (10-75 g/cm^3), and inhalation rate (L/min). Map was constructed based on data from Tables 5-8

When insertion angle, particle density and inhalation rate were varied, particle deposition appeared to still remain most sensitive to inhalation rate (Fig 7). As evidenced by the random array of colors, there was no notable consistent variation in the pattern of deposition with respect to the insertion angle parameter (Fig 7).

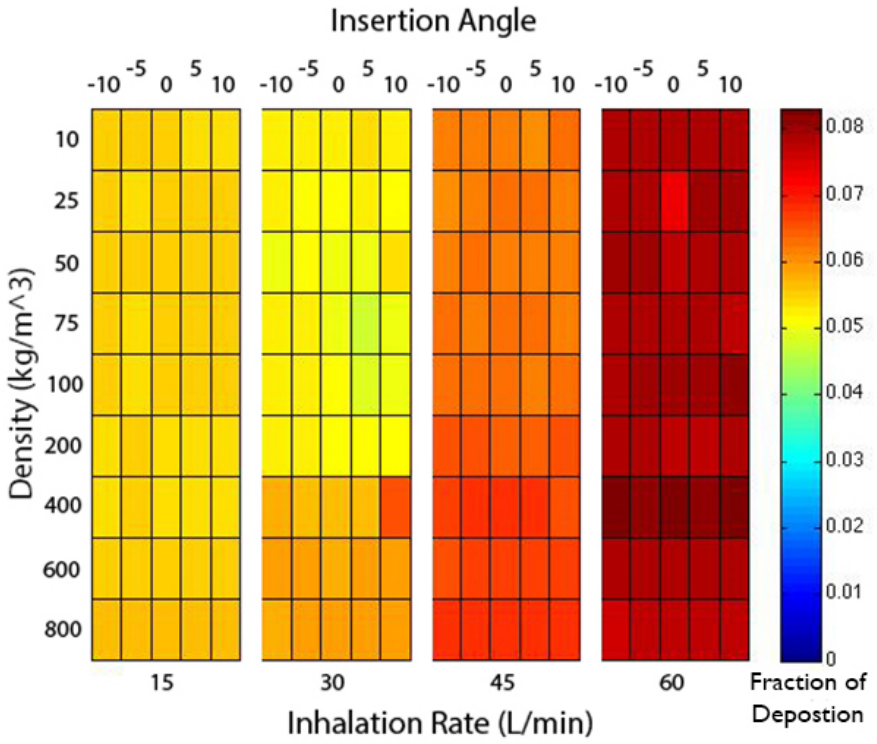

Figure 7. Heat map of deposition fraction of insulin particles as a function of particle diameter (µm), particle density (g/cm^3), and inhalation rate (L/min) based on data from Tables B13-16

3.2 2D Turbulent Model

3.2.A Velocity Profile

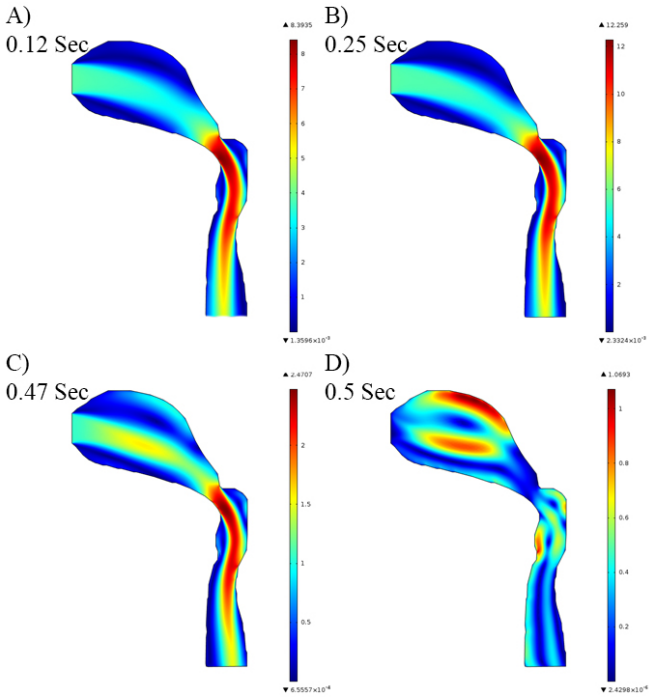

Figure 8. 2D Turbulent velocity profiles for time range (0:0.01:0.5s) at the following time points: (A) t = 0.12s (B) t = 0.25s (C) t = 0.47s (D) t = 0.5s

The velocity profile pattern over time for the turbulent model is very similar to that of the laminar model. The velocity increases to a peak velocity of 12.3 m/s at 0.25 s (Fig 8B) and then decreases substantially after that. Velocities are consistently higher in the trachea compared to the oral cavity (Fig 8B, 8C). The narrow diameter of the trachea is characteristic of a "bottle-neck" region and results in a significant increase in flow velocity (Fig 8A, 8B). A unique characteristic of the velocity profile in the Turbulent Model shown for the final time step (t = 0.5 s) is the presence of a flow vortex in the oral cavity (Fig 8D).

3.2.B Particle Tracing

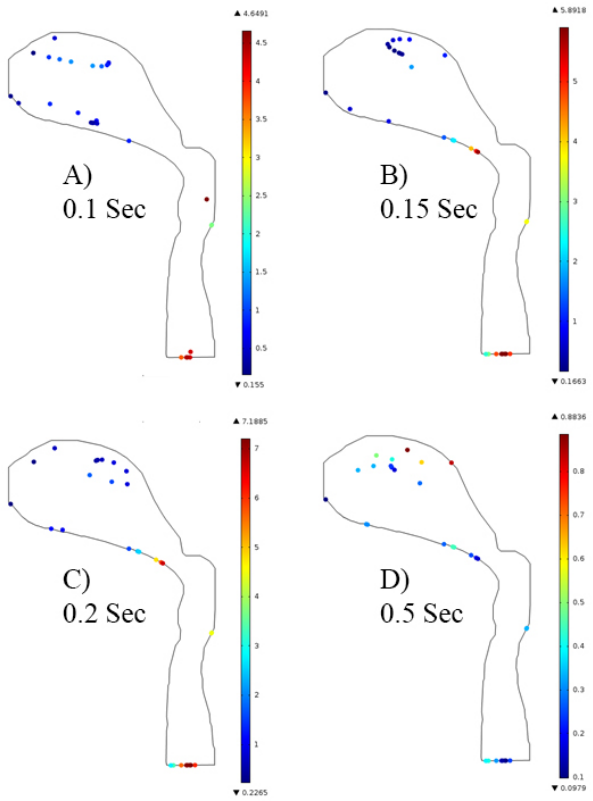

Figure 9. Particle trajectory plots in 2D turbulent flow for time range (0:0.01:0.5) at the following time points: (A) t = 0.1s (B) t = 0.15s (C) t = 0.2s (D)t = 0.5s

As with the laminar model, particle trajectories in the turbulent model change over time (Fig 9). However, particles progress through the cavity faster in the turbulent model. At the first time point (t = 0.1s), particles are just entering the oral cavity in the laminar model (Fig 9A), but there is already particle deposition in the turbulent model (Fig 9A). The velocity of particles tends to decrease as they continue their pathway down the trachea, which demonstrates the effect of particle impaction against the pharynx wall (Fig 9D). At the middle time points (t= 0.15 and 0.2s), there appears to be particles in the upper region of the oral cavity moving circularly, which may indicate the presence of a flow vortex (Fig 9C, 9D).

3.2.C Particle Deposition

Varying inhalation rate, particle diameter and density appeared to have no effect on particle deposition (Fig 10). While the laminar model showed a direct relationship between particle deposition and inhalation rate, for the Turbulent Model, the deposition for all inhalation rates is comparable. Additionally, the fraction of particles deposited in the turbulent model is about a magnitude smaller than that of the 2D laminar model (Fig 5). The fraction of particles deposited ranged from 0 to 0.02 for the turbulent model and 0.048 to 0.08 for the laminar model for the same densities tested (Fig 10, 5).

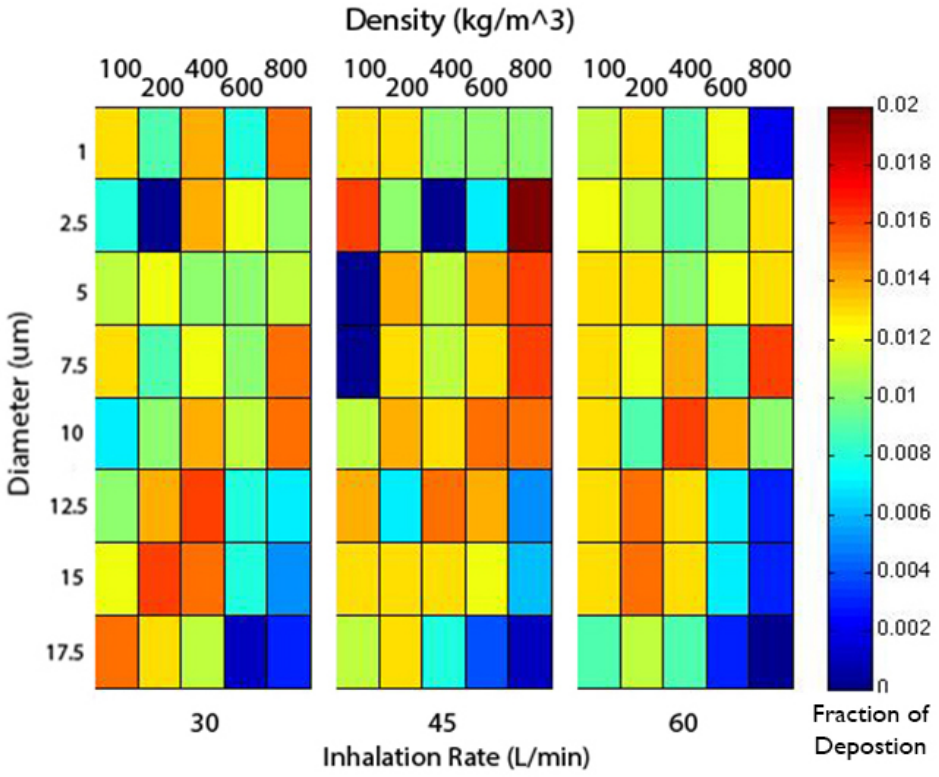

Figure 10. Color intensity map of 2D turbulent flow deposition fraction of insulin particles as a function of particle diameter (µm), particle density (g/cm^3), and inhalation rate (L/min) based on data from Tables B5-8, B13-16.

We believe that this decreased deposition occurred because of turbulent dispersion effects present in the oral cavity in the turbulent model. As indicated in (Fig 11) by the black circle, this flow vortex traps particles near the top boundary of the oral cavity. Particles trapped in this vortex move continuously along the vortex edges, where shear stress and air velocity are high, which negatively affects particle deposition at the bottom of the trachea[12].

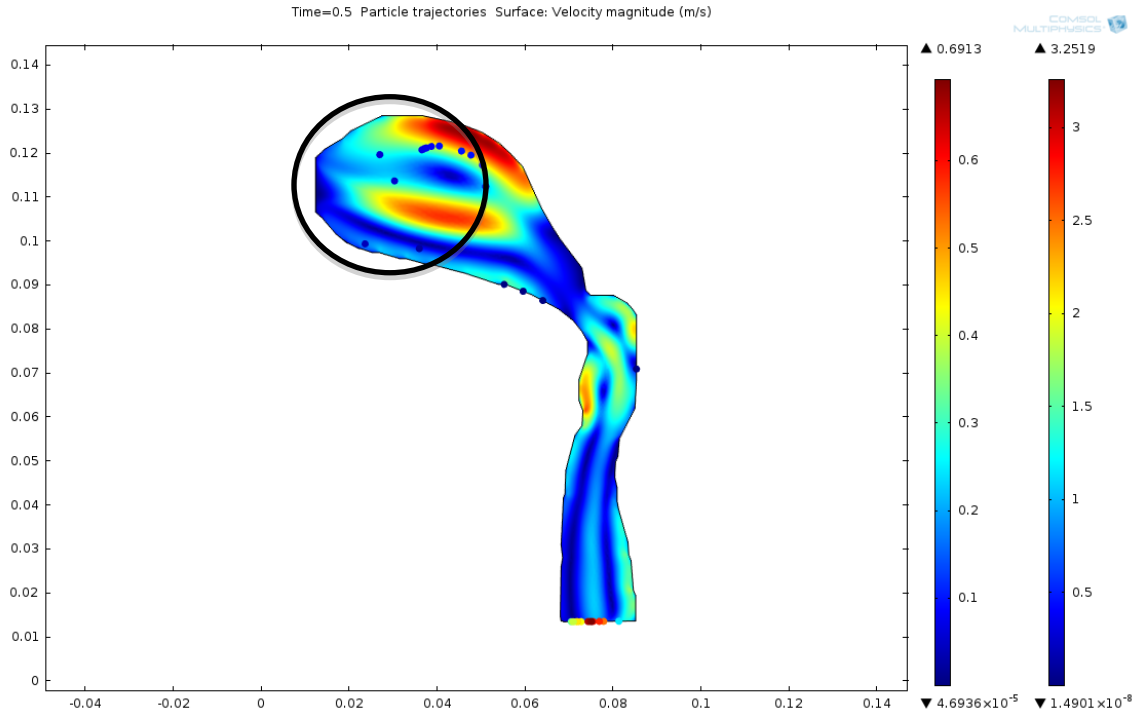

Figure 11. Time = 0.5 seconds at 30 L/min 2D turbulent flow, particle diameter = 1µm, and particle density = 400 g/cm^3. This figure indicates how particles are be trapped in the vortex show in the black circle above. The flow vortex accounts for the low particle deposition for turbulent flow.

Although the presence of a flow vortex in the turbulent model may explain low particle deposition, the absence of any correlation between the tested parameters of inhalation rate, particle density and diameter in relation to the extremely low particle fraction deposition should be interpreted with caution. It is possible that the COMSOL solver was solving within an error range due to the physics associated with the extreme complexity of turbulent flow, the number of particles entering the cavity being too small, or the particles being micro-sized.

3.3 3D Laminar Model

3.3.A Velocity Profile

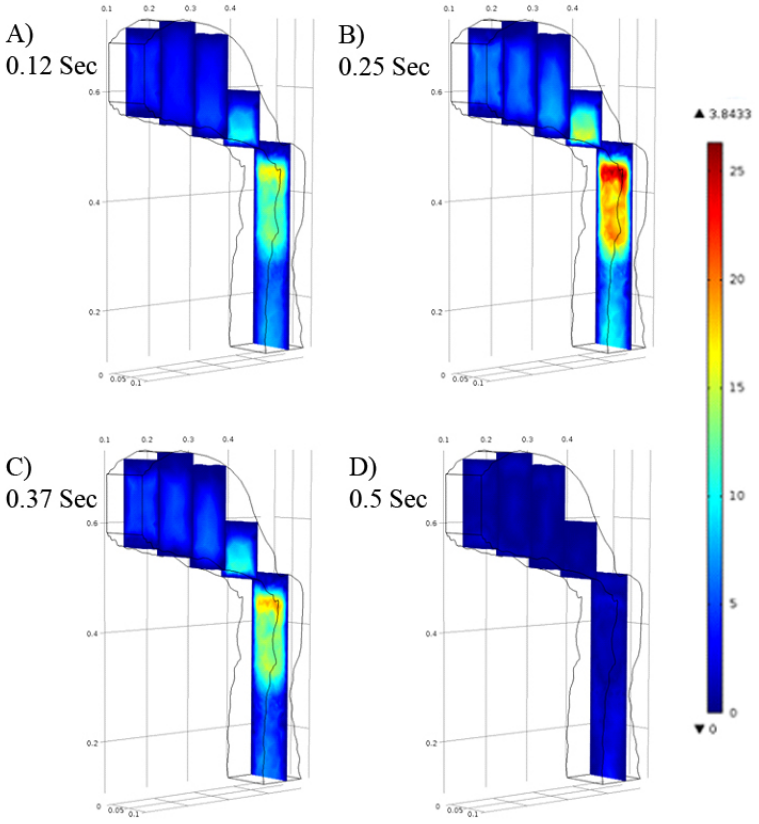

Figure 12. Velocity Profiles for time range (0:0.01:0.5s) at the following time points: (A) t = 0.12s (B) t = 0.25s (C) t = 0.37s (D) t = 0.5s from five yz-planes.

The velocity profile pattern over time in the 3D model was congruent with the previous 2D model results. Velocity profiles were observed by taking five cross-sectional yz-planes (Fig 12) and eight cross-sectional xz-planes (Fig 13) throughout the geometry for an inhalation rate of 60 L/min. Air flow velocities increased with time to a maximum velocity observed at t = 0.25 s. After the peak velocity at t = 0.25 s, air flow velocities decreased due to the sine-wave function specified at the inlet velocity. Similarly to the 2D model, the 3D model also displayed a "bottle-neck" region resulting in a high concentration of higher velocities in the constricted area by the pharynx. Velocities in the trachea were overall higher in the trachea due to the reduced area, which is consistent with our 2D model. Due to the consistent pattern of the airflow with the 2D model and small variation of velocities in the z-axis at the given time scales, the 2D model assumption may be accurate and appropriate for laminar flow. Most of the variation in the velocities in the z-direction occurs in the trachea at t = 0.25 s, with the center of the trachea having higher velocity airflow than the edges.

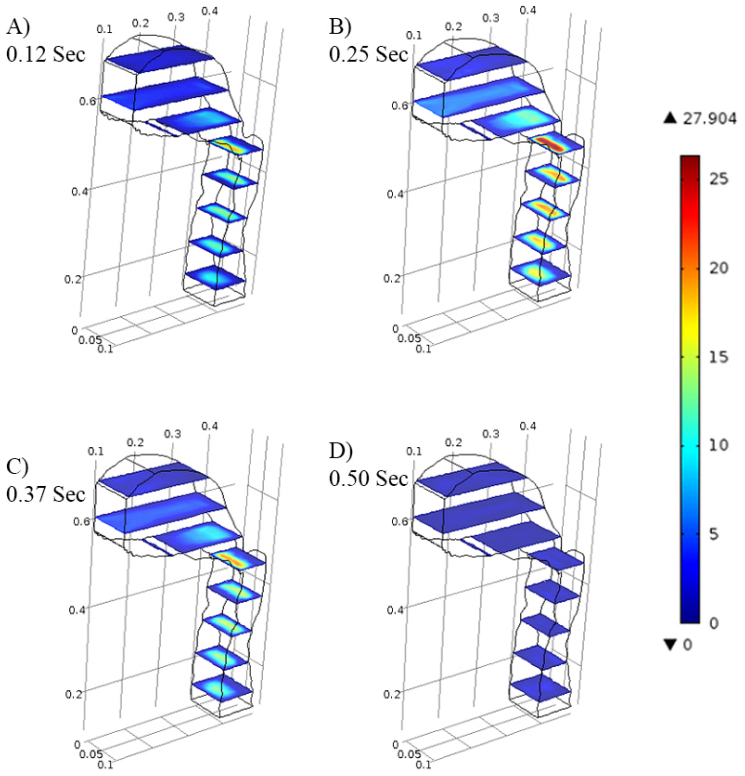

Figure 13. Velocity Profiles for time range (0,0.01,0.5s) at the following time points: (A) t=0.12s (B) t=0.25s (C) t=0.37s (D) t=0.5s from eight xz-planes.

3.3.B Particle Tracing

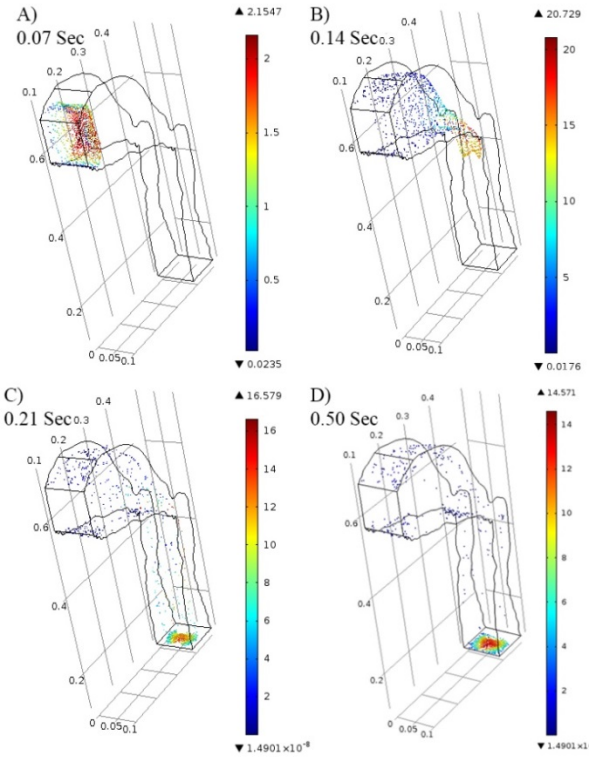

Figure 14. 3D particle trajectory plots for time range (0:0.01:0.5s) at the following time points: (A) t = 0.07 s (B) t = 0.14 s (C) t = 0.21 s (D) t = 0.50s.

One thousand particles were specified at the inlet with uniform distribution with an inhalation rate of 60 L/min, particle diameter of 1 µm, and particle density of 200 kg/m^3. The particle trajectory pattern in the 3D model agreed well with the particle trajectory pattern in the 2D model. Particles entering the oral cavity at t = 0.07 s closely followed the airflow, forming a ring of particles that travelled outward as the airflow propelled forward from the inlet (Fig 14A). Particles with the highest velocities were found at the center of the oral cavity where the highest airflow velocities were also found. A short time later, higher velocities for the particles were observed in the trachea, which is consistent with the velocity profiles and the 2D model (Fig 14B). Particles then deposited at the bottom of the trachea, as desired by the design objectives, with high velocities (Fig 14C). Other particles deposited at the oral cavity wall near the inlet in both the top and bottom layers with low velocities.

3.3.C Particle Deposition

The particle deposition pattern in the oral cavity walls was fairly uniform in the z-direction (Fig 14D), while particles at the bottom of the trachea formed a circle of higher concentration of particles towards the center where the airflow was presumably higher from the xz-plane velocity plots. The total particle deposition at the bottom of the trachea, represented as the bottom outlet plane, was quantified to be 681 particles of the 1,000 particles at the inlet

(68.1%). The particle deposition rate in 3D laminar flow at the bottom of the trachea was larger than the corresponding particle deposition in the 2D laminar flow model by a factor of 8.

The difference in the deposition rate in the 3D laminar model may be a result of a number of factors that are different from the 2D laminar model. First, the absence of the mucus layers of higher viscosity that slowed down particles in the 2D model may be a factor in the higher deposition rates. One thousand particles were used in the 3D model with a significantly larger volume in the geometry, compared to 10,000 particles in the 2D model for a facilitated computing process. Furthermore, a total of 5 particles (0.5%) deposited on the lateral boundaries layers of the geometry. The top and bottom layers of the oral cavity had a total of 84 particles deposit (8.4%). The larger volume in the oral cavity available for particle transport in the 3D laminar model reduces deposition on the oral cavity walls before the particles reach the bottom of the trachea as the laminar flow is fairly uniform and the highest velocities are concentrated towards the center of the airflow. A turbulent model may be more accurate in the 3D model for higher inhalation rates as it captures the effect of turbulence, such as vortex stretching, more fully than the 2D turbulent model does and may yield higher particle deposition rates in the oral cavity wall as a result [14].

3.4 Accuracy Check

3.4.A Laminar Velocity Profiles

The velocity profile was obtained for a cutline designated from point (0.0651, 0.0746) to point (0.0786, 0.0925) by averaging the velocities over time for three different flow rates: 15 L/min, 30 L/min, and 90 L/min. The velocities were then normalized by dividing by the initial inlet velocity value (Fig 15). The data was compared against experimental and computational fluid dynamic model results from a study by Heenan et al. (2003) (Fig 16) [6]. The general trend of the curves is a sharp velocity increase from the left boundary, a relatively flat region towards the center, and a sharp decrease in velocity towards the right boundary is consistent with literature data (Fig 16) [6]. Furthermore, the peak normalized velocity values of 1.53 for the 15 L/min flow rate, 1.37 for the 30 L/min flow rate, and 1.27 for 90 L/min agree with the experimental values recorded by Heenan et al (Fig 15)[6]. The normalized data values obtained from this model are more consistent with the experimental data than the CFD model from Heenan et al, especially for the lower flow rates.

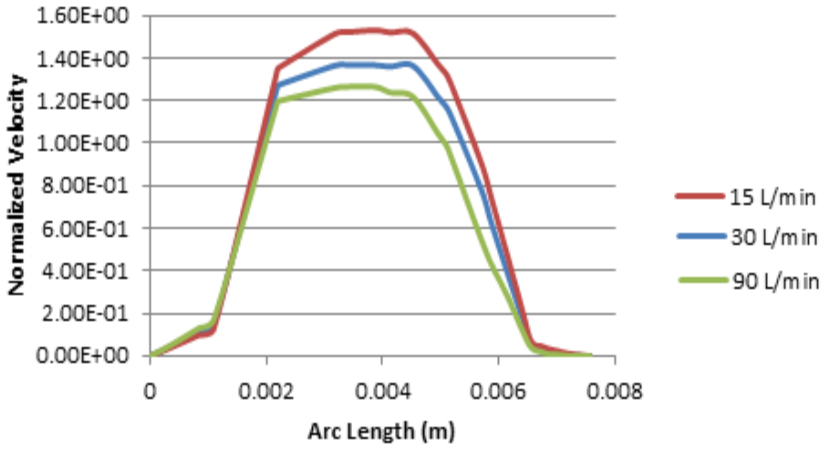

Figure 15. Velocity profile averaged over time for 15 L/min, 30 L/min, and 90 L/min for cutline from point (0.0651, 0.0746) to point (0.0786, 0.0925).

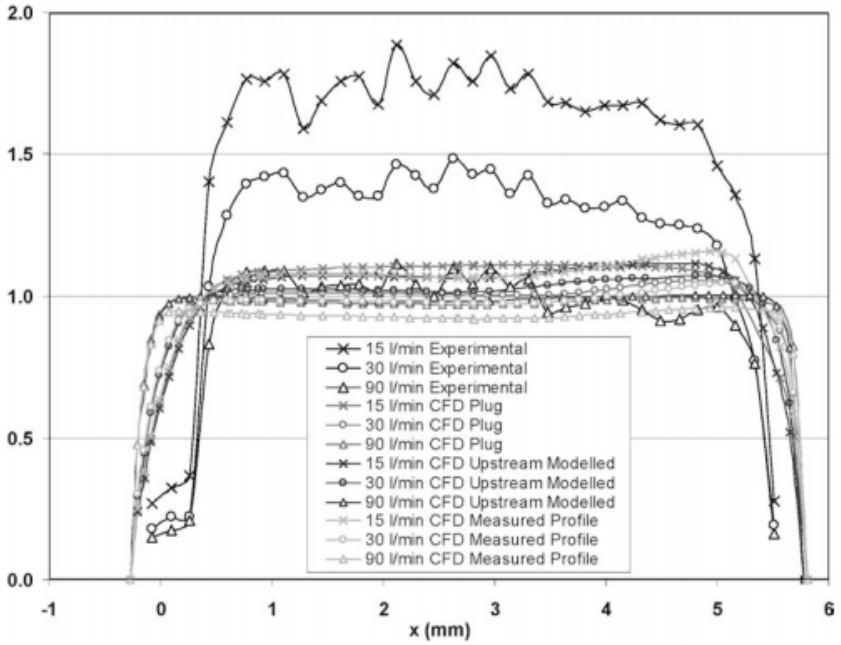

Figure 16. Normalized velocity profile averaged over time (Imaged adapted from [6]).This figure shows congruence with our velocity profile averaged over time (Fig 15), showing that our model had a reasonable level of accuracy.

3.4.B Laminar Deposition Results

Bronsky et al. studied the effects of peak inspiratory aerolizer flow rates for the use of inhalers[11].They had found that lower inspiratory rates (<30 L/min) not only prevented the aerosolization of particles, but decreased pre-aerosolized particle deposition into the lungs. Higher inspiratory rates (>60L/min) were found to increase aerosolization and deposition into the lungs.

A study by Heyder demonstrated a consistent trend that particles with larger diameters reached the bottom of the trachea less effectively for particle diameter sizes in the range of 1-10 µm, which was a pattern found in our results for the larger laminar inhalation rates[13]. In addition to particle diameter, the study also found that particles with greater density deposited onto to the oral cavity wall at higher rates without reaching the bottom of the trachea[13]. The particles with larger diameter and density showed increased deposition onto the oral cavity walls through impaction, which reduced the number of particles reaching the bottom of the trachea.

3.5 Sensitivity Analysis

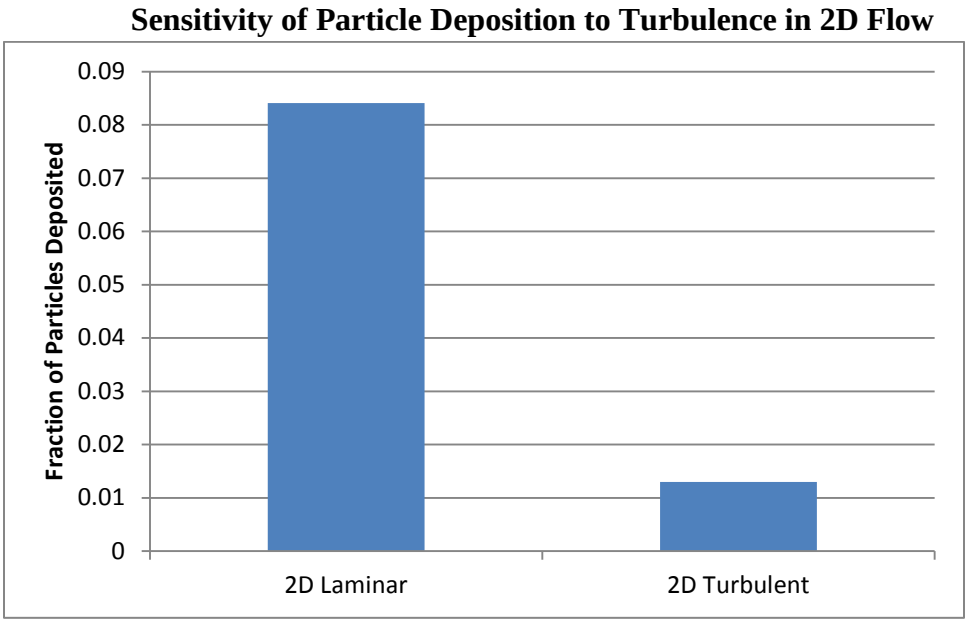

Figure 17. Sensitivity of particle deposition to turbulence in 2D flow. The figure shows that there is a very large difference between the deposition fractions for the two models.

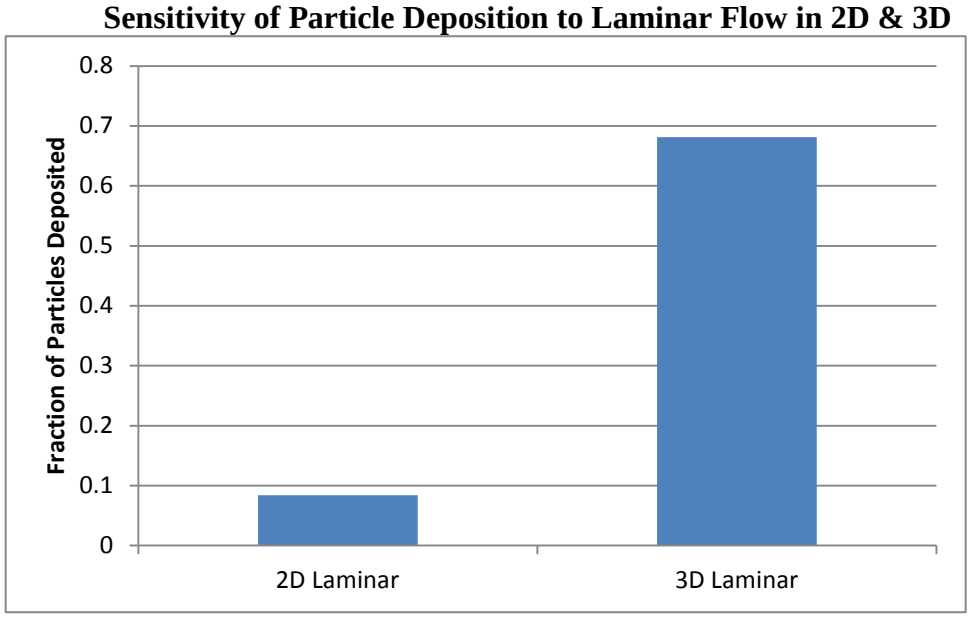

Figure 18. Sensitivity of particle deposition to laminar flow in 2D and 3D. The figure shows that there is a very large difference between the deposition fractions for the two models.

Sensitivity analysis was conducted by examining how using our 2D turbulent and 3D laminar would affect our particle deposition at the bottom of the trachea. For the analysis, we standardized the particle diameter at 1 μm, the particle density at 200 kg/m^3, and the inhalation rate at 60 L/min. Looking at the 2D turbulent results in comparison to the 2D laminar results (Fig 17), the deposition rates were smaller than our original 2D laminar model (1.3% in turbulent vs. 8.4% in laminar). This is most likely caused by the trapped particles in the vortices found in the upper part of the oral cavity. These vortices are caused by the dispersion of kinetic energy based on the turbulent governing equations used. When comparing the 2D laminar results to the 3D laminar results (Fig 18), the deposition rates were significantly higher than the 2D laminar results (68% in 3D vs. 8.4% in laminar). By increasing the 2D model to 3D, you are increasing the free area for the particles from x^2 to $A*x^3$, while the particles to be trapped on the oral cavity surface from x to $B*x^2$. We believe that the increased degree of freedom for movement in the oral cavity increased the particle deposition.

4. Conclusion & Design Recommendations

4.1 Conclusion

The 2D laminar flow model demonstrated the direct relationship between inhalation rate and particle deposition in the tracheal region. The model was most sensitive to inhalation rate compared to the other experimental parameters. The laminar study indicated that at high inhalation rates (45-60 L/min), particles with low density (100-400 kg/m^3) and low diameter (1-7.5 micrometers) resulted in increased particle deposition. Even when the insertion angle of the inhaler was varied, the model still remained most sensitive to changes in inhalation rate. These results agree with literature, which shows that at high inhalation rates, particles with large diameters and densities are less likely to be deposited at the bottom of the trachea[13].

Varying inhalation rate, particle density and diameter appeared to have no significant effect on particle deposition for the 2D turbulent flow model. The 2D turbulent model displayed particle depositions that were an order of a magnitude lower than those of the 2D laminar model. This decreased deposition can be explained by turbulent dispersion effects present in the model, with particles becoming trapped in a flow vortex in the oral cavity. Nevertheless, the random pattern in particle deposition indicates that there are problems associated with our implementation in COMSOL associated with the increased complexity of turbulent flow.

The velocity profiles and particle trajectories in the 3D laminar model qualitatively were in good agreement with the 2D laminar velocity profiles and particle trajectories. Velocity profiles and particle deposition patterns in the oral cavity were fairly uniform in the z-direction, indicating that a 2D laminar assumption may be accurate in this region. The center of the pharynx and trachea showed higher velocities and subsequent higher deposition of particles in the center of the bottom of the trachea.

4.2 Implications & Relevance

Our model demonstrates the importance of how the combinations of several factors have an effect on drug particle deposition. While inhalation rate was deemed to be the most sensitive parameter for particle deposition, there were slight differences in results when a range of particle diameters and densities were implemented. Thus, when formulating oral drug treatment particles, the various particle characteristics should be formulated with specific inhalation rates in mind. Using our model, it is possible to dictate whether a treatment involving oral inhalation drug delivery method can fit within the parameters required for optimal deposition.

4.3 Design Recommendations

Based on our 2D laminar study results, we determined that effective particle deposition was achieved at high inhalation rates (45-60 L/min), low density (100-400 kg/m^3) and low particle diameters (1-7.5 micrometers). Therefore, we would recommend designers of oral inhalers to focus on these three parameters: inlet velocity, particle diameter, and particle density.

In terms of the model design, the turbulent model results indicated that the type of airflow selected had a significant effect on the particle deposition pattern. Changes in particle diameter, particle density, and inhalation rate parameters did not display a clear trend of effects on particle deposition at the bottom of the trachea for the turbulent model. Furthermore, while the general

pattern of airflow and particle trajectories were similar in the 3D to the 2D model, higher deposition rates were observed in the 3D model than the 2D laminar model. As a design recommendation, we suggest implementing the mucus layer to the 3D geometry to quantify the effects of the mucus layer on particle velocities and particle deposition at the bottom of the trachea. In addition, we recommend implementing turbulent flow in a 3D model for higher inhalation rates. Turbulent flow models are most realistic in 3D as the full extent of vortex stretching and other turbulent-flow characteristics can be implemented[12]. The turbulent airflow with subsequent turbulent dispersion of particles in 3D may yield a more realistic implementation of the relevant physics and help identify other parameters involved in the turbulent dispersion process.

One of the main limitations associated with our model was the tracheal cut off boundary. For simplification purposes, the model of our oral cavity did not include the lower peripheral airways. Thus, it was assumed that particle deposition at the tracheal cut off boundary was equivalent to the particle deposition in the lungs. Thus, we recommend extending the model from the bottom of the trachea to include the bronchi and the lungs. A complete geometry of the respiratory system will allow for better quantification of bioavailable particle deposition directly on the surface of the lungs. Additionally, the 3D geometry was an extrusion of the 2D geometry in the z-direction. Ideally, we would recommend a more realistic geometry with smoother, more cylindrical outlines and overall shape. Furthermore, our model does not include biological variation to account for changes in the oral cavity based on factors such as gender and age.

4.4 Realistic Constraints

The constraints involved with implementing our model include cost, dosage flexibility, and safety. The average wholesale price of inhaled insulin is significantly higher (approximately $125) than that of insulin injection therapy[14]. Nevertheless, after analysis of customer requirements, the benefits associated with increased patient satisfaction with inhaled insulin may be deemed more important than the high cost. Additionally, any changes made to the insulin dosage, such as the rate at which particles are inhaled and particle size, need to be tested using clinical trials on numerous patients to ensure the dosage's safety and effectiveness[14]. Lastly, although inhaled insulin is a promising alternative to injection therapy, it has some side effects that need to be examined further, including increased concentrations of insulin antibodies[15]. More research is needed to confirm the safety of inhalable insulin before it is fully utilized in a large scale.

APPENDIX A: Mathematical Model

A1. Mesh

2D Mesh

An unstructured extremely fine mesh was applied to the schematic of the human oral cavity (Fig 2) to create a mesh structure consisting of 14,761 triangular elements for the laminar model (Fig 3). The mesh element size was calibrated for the general physics of the model; a higher density of elements were specified in regions with the highest velocity and particle trajectory changes, which included the inlet, pharynx, and trachea. The turbulent model featured a similar physics-based finer mesh with 19,337 elements (Fig 3).

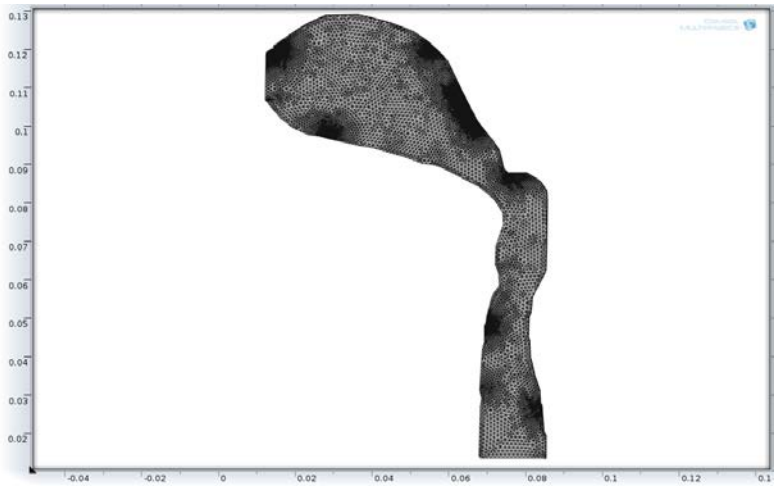

Figure A1. Unstructured extremely fine mesh for laminar model consisting of 14,761 triangular elements created for the oral cavity schematic.

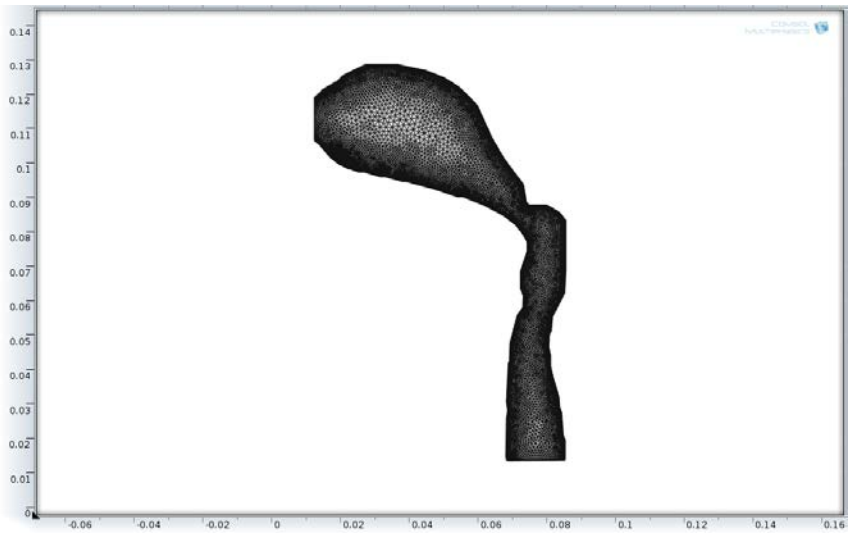

Fig A2: Physics-controlled finer mesh consisting of 19,337 triangular elements created for the turbulent model.

3D Mesh

An unstructured finer mesh was applied to the schematic of the human oral cavity to create a mesh structure consisting of 29,796 tetrahedral elements (Fig 4).

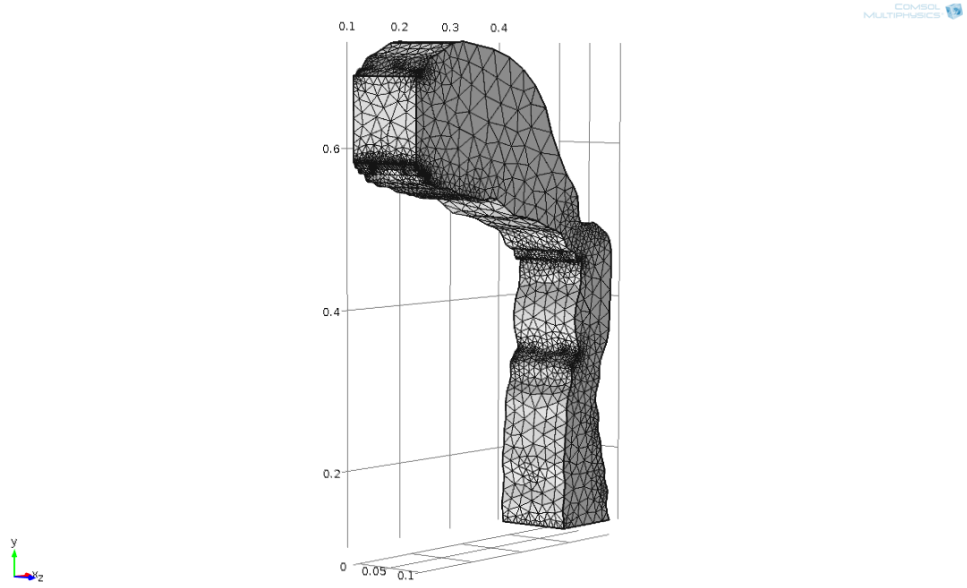

Figure A3. Unstructured finer mesh consisting of 29,796 tetrahedral elements created for the 3D oral cavity geometry.

A2. Governing Equations

2D Laminar Model

Oral drug delivery through inhalation was modeled as 2D laminar flow using the Navier-Stokes equation for momentum conservation and the continuity equation for conservation of energy. Lagrangian particle tracing equations were used for tracking particle velocity and location.

Continuity:

$$\frac{\partial \rho}{\partial t} + \frac{\partial(\rho u)}{\partial x} + \frac{\partial(\rho v)}{\partial y} = 0$$

Navier-Stokes:

$$\rho\left(\frac{\partial u}{\partial t} + u\frac{\partial u}{\partial x} + v\frac{\partial u}{\partial y}\right) = -\frac{\partial p}{\partial x} + \mu\left(\frac{\partial^2 u}{\partial x^2} + \frac{\partial^2 u}{\partial y^2}\right) + \rho g_x$$

$$\rho\left(\frac{\partial u}{\partial t} + u\frac{\partial u}{\partial x} + v\frac{\partial u}{\partial y}\right) = -\frac{\partial p}{\partial y} + \mu\left(\frac{\partial^2 u}{\partial x^2} + \frac{\partial^2 u}{\partial y^2}\right) + \rho g_y$$

Lagrangian Particle Tracing for Particle Velocity and Location:

$$m_p \frac{\delta u_p}{\delta t} = [F_d(u_g - u_p)]m_p$$

$$F_d = \frac{18\mu_g C_d Re_p}{24\rho_p d_p^2}$$

$$Re_p = \rho_p d_p \frac{|u_p - u_g|}{\mu_g}$$

2D Turbulent Model

The momentum equation is a time-averaged equation of motion derived from the 2D Navier-Stokes equation for fluid flow. The Reynold's number for our model at an inhalation rate of 60 L/min, a flow diameter of 0.015 m, and the dynamic viscosity and density of air was calculated to be 8,805. This low Reynold's number justified our use of the k-ω turbulence model of laminar-to-turbulent two-phase flow, which includes the turbulent kinetic energy and pseudo-vorticity equations[1]. The k-ω model solves for the rate at which the dissipation of turbulent kinetic energy occurs[1].

Momentum equation

$$\frac{\partial \bar{u}_i}{\partial t} + \bar{u}_j \frac{\partial \bar{u}_i}{\partial x_j} = -\frac{1}{\rho}\frac{\partial p}{\partial x_i} + \frac{\partial}{\partial x_j}[(v + v_T)(\frac{\partial \bar{u}_i}{\partial x_j} + \frac{\partial \bar{u}_j}{\partial x_i})$$

Turbulent kinetic energy (k) equation

$$\frac{\partial k}{\partial t} + \bar{u}_j \frac{\partial k}{\partial x_j} = \tau_{ij}\frac{\partial \bar{u}_i}{\partial x_j} - \beta^* k\omega + \frac{\partial}{\partial x_j}[(v + \sigma_k v_T)\frac{\partial k}{\partial x_j}]$$

Pseudo-vorticity (ω) equation

$$\frac{\partial \omega}{\partial t} + \bar{u}_j \frac{\partial \omega}{\partial x_j} = \alpha\frac{\omega}{k}\tau_{ij}\frac{\partial \bar{u}_i}{\partial x_j} - \beta\omega^2 + \frac{\partial}{\partial x_j}[(v + \sigma_\omega v_T)\frac{\partial \omega}{\partial x_j}]$$

3D Laminar Model

The 3D model utilized the expanded the governing equations in the 2D laminar flow model to include thez-axis. The governing equations used were the continuity equation, Navier-Stokes, and Lagrangian particle tracing for particle velocity and location.

Continuity in 3D:

$$\frac{\partial \rho}{\partial t} + \frac{\partial (\rho u)}{\partial x} + \frac{\partial (\rho v)}{\partial y} + \frac{\partial (\rho w)}{\partial z} = 0 \quad \frac{\delta \rho}{\delta t} + \frac{\delta (\rho u)}{\delta x} + \frac{\delta (\rho v)}{\delta y} + \frac{\delta (\rho w)}{\delta z} = 0$$

Navier-Stokes in 3D:

$$\rho \left(\frac{\partial u}{\partial t} + u\frac{\partial u}{\partial x} + v\frac{\partial u}{\partial y} + w\frac{\partial u}{\partial z} \right) = -\frac{\partial p}{\partial x} + \mu \left(\frac{\partial^2 u}{\partial x^2} + \frac{\partial^2 u}{\partial y^2} + \frac{\partial^2 u}{\partial z^2} \right) + \rho g_x,$$

$$\rho \left(\frac{\partial v}{\partial t} + u\frac{\partial v}{\partial x} + v\frac{\partial v}{\partial y} + w\frac{\partial v}{\partial z} \right) = -\frac{\partial p}{\partial y} + \mu \left(\frac{\partial^2 v}{\partial x^2} + \frac{\partial^2 v}{\partial y^2} + \frac{\partial^2 v}{\partial z^2} \right) + \rho g_y$$

$$\rho \left(\frac{\partial w}{\partial t} + u\frac{\partial w}{\partial x} + v\frac{\partial w}{\partial y} + w\frac{\partial w}{\partial z} \right) = -\frac{\partial p}{\partial z} + \mu \left(\frac{\partial^2 w}{\partial x^2} + \frac{\partial^2 w}{\partial y^2} + \frac{\partial^2 w}{\partial z^2} \right) + \rho g_z$$

A3. Boundary Conditions

Flow Boundary Conditions

- Oral cavity wall is rigid
    - The 2D Laminar model included a mucus layer with consistent thickness of 0.1 m throughout cavity wall[9]
- No slip condition for fluid at the mucus boundary layer for the 2D laminar model
- Pressure at inlet and outlet is 0 for 2D turbulent model
- "Stick" condition
- Average inhalation rate ranges from 15 L/min to 60L/min
    - Inhalation was based on a sine function

Diffusion boundary Condition

- Oral cavity wall is impermeable to drug flow

A4. Assumptions

Fluid Flow

- Laminar airflow for the 2D & 3D laminar models and turbulent airflow for the 2D turbulent model
- Incompressible and Newtonian fluid

Particles

- Particles acted upon by gravitational force, which was defined as a gravity vector (0, -9.81 m/s^2)
- Particles upon by drag force defined by Stoke's Law (predefined in COMSOL)
- Particles are of uniform spherical sizes
- For the turbulent model, particle deposition was not computed to the last time step due to computing limitations. For these parameter combinations, the particle deposition at the last computed time step was assumed to be the particle deposition.

A5. Input Parameters

2D Laminar Input Parameters

Table A1. Fluid properties for the various domains in the COMSOL model[16]

Fluid	**Air**	**Water**
Domain	Oral cavity	Mucous layer
Density (g/m^3)	1.225	1000
Dynamic Viscosity (Pa*s)	1.181×10^{-5}	8.9×10^{-4}

Table A2. Input parameters and variables. Parametric sweep analysis was completed by computing all combinations of particle density (g/m^3), particle diameter (μm), and inhalation rate (m/s). The lower half of the table indicates the velocity parameters implemented into the model. The Laminar Flow module of the model uses an inhalation rate that is a function of time. Implementing inhalation rates into our 2D COMSOL model required that the volumetric flow rates (L/min) obtained from literature be converted a velocity rate (m/s). An approximation of the inlet oral cavity cross sectional area was used for this conversion. The inlet oral cavity was assumed to be a circle geometry, and the cross sectional area in the model was approximated as $\left(\pi r^2 = \pi\left(\frac{0.015\,m}{2}\right)^2 = 1.77 * 10^{-4} m^2\right)$ [5]. The Particle Tracing module of the model uses initial particle velocities that were calculated based on the assumption that inhalers are frequently used at an angle θ with respect to the horizontal[2].

# Particles[17]	10000							
Particle Density (g/m^3) [17]	100	200		400		600		800
Particle Diameter (μm) [17]	1	2.5	5	7.5	10	12.5	15	17.5
Insertion Angle (θ)[2]	-10°	-5°		0°		5°		10°

(Laminar Flow Module) Inhalation Rate[11]		
Volumetric Flow Rate (L/min) [11]	*Velocity Rate, v (m/s)*	*Inhalation Rate = f(t)*
15	1.415	v*sin (2π*t)
30	2.830	
45	4.244	
60	5.659	

(Particle Tracing Module) Initial Particle Velocity (m/s)[1]	
u_x	1.415
u_y	1.415*Sinθ

2D Turbulent Input Parameters

Table A3: Input parameters and variables. Parametric sweep analysis was completed by computing all combinations of particle density (g/m^3), particle diameter (μm), and inhalation rate (m/s). There were a few implementation differences in running the turbulent model compared to running the laminar model. Firstly, particle deposition was not examined at an inhalation rate of 15 L/min, as the model did not compute with this condition. This result can be explained by the turbulence intensity being very low[12]. At this low flow rate condition, inlet turbulence is diminished and laminar flow prevails[12]. Additionally, the number of particles entering the mouth was decreased from 10,000 to 1,000, as the turbulent model did not compute when the higher particle number was set. This discrepancy may have occurred due to the increased complexity associated with flow through the turbulent model.

# Particles[17]	1000							
Particle Density (g/m^3) [17]	100		200		400		600	800
Particle Diameter (μm) [17]	1	2.5	5	7.5	10	12.5	15	17.5
(Turbulent Flow Module) Inhalation Rate[11]								
Volumetric Flow Rate (L/min) [11]	*Velocity Rate, v (m/s)*				*Inhalation Rate = f(t)*			
30	2.830				v*sin (2π*t)			
45	4.244							
60	5.659							
(Particle Tracing Module) Initial Particle Velocity (m/s)[1]								
u_x	1.415							
u_y	-0.249							

Two additional parameters specific for the turbulent model include the turbulence length scale, which was set to 1, and the turbulence intensity, which was set to 10% [12].

APPENDIX B: Solution Strategy

B1. Mesh Convergence

Velocity

Mesh convergence was performed for laminar flow velocities at a cross section in the oral cavity at time t=0.25s. The cross section was defined from point (0.0651, 0.0746) to point (0.0786, 0.0925) (Fig 5). For meshes with a fewer number of elements, the velocity distribution across arc length curve was not that "smooth" (Fig 6). As the mesh was refined, the velocity distribution across arc length "smoothens" out and becomes less jagged (Fig 6). Eventually, the velocity distribution no longer changes with mesh refinement at approximately 16181 elements, and mesh convergence has been accomplished. It was also observed that the velocity of airflow was significantly decreased at the junction of oral cavity wall and mucosal layer (Fig 6). This was evidenced in sharp velocity reductions at the lower and upper arc length values (Fig 6).

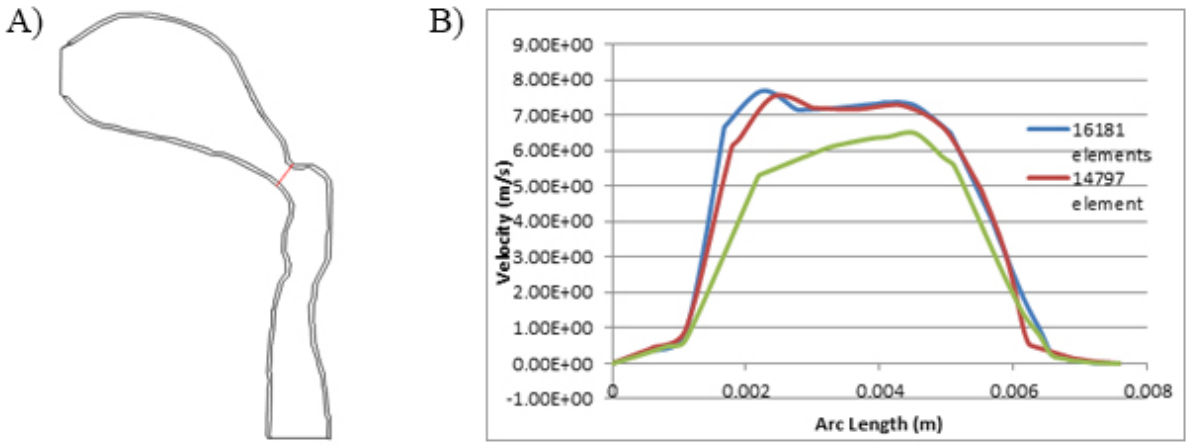

Figure B1. A) Cutline region designated from point (0.0651, 0.0746) to point (0.0786, 0.0925) for velocity profile B) Mesh convergence for laminar flow velocity profiles.

Particle Trajectory

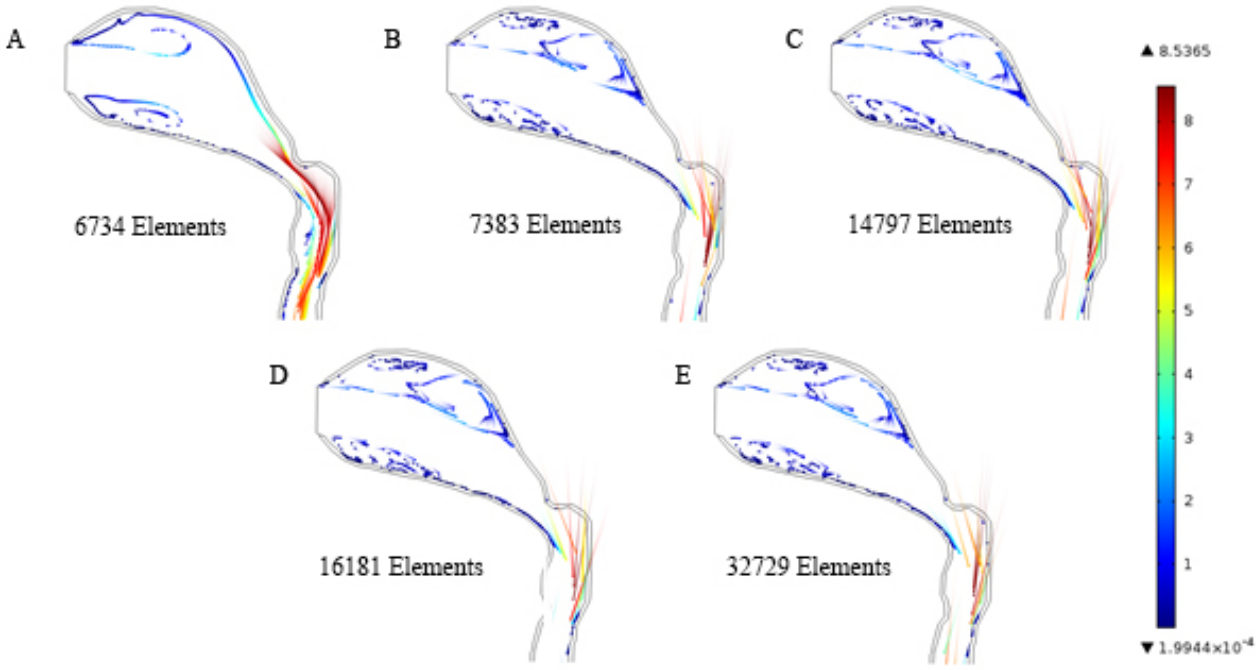

Figure B2. Particle trajectory plots for different mesh sizes at time = 0.13 sec for various maximum element size (M_E). (A) M_E = 0.0427 m (B) M_E = 0.00231 m (C) M_E = 0.00115 m (D) M_E = 0.00075 m (E) M_E = 0.0005 m

Mesh convergence was accomplished for particle trajectories. This is evidenced as the solution becomes independent of the mesh as the mesh becomes more refined. The changes in the solution between a complete mesh containing 14,797 and 16,181 number of elements become insignificant (Fig 7D, 7E). As number of mesh elements increases, and thus the mesh is refined, the solution becomes independent of the mesh discretization (Fig 7).

B2. Particle Deposition Data

2D Laminar

Table B1. 2D Laminar particle deposition at tracheal boundary for particle diameters and lower particle densities at an inhalation rate of 15 L/min.

Inhalation rate = 15 L/min		**Particle Density (g/cm^3)**			
		10	*25*	*50*	*75*
Particle Diameter (µm)	*1*	0	544	545	541
	2.5	541	542	543	543
	5	543	540	543	545
	7.5	544	548	542	549
	10	547	543	544	543
	12.5	544	547	546	543
	15	551	545	549	544
	17.5	549	544	545	547

Table B2. 2D Laminar particle deposition at tracheal boundary for particle diameters and lower particle densities at an inhalation rate of 30 L/min.

Inhalation rate = 30 L/min		**Particle Density (g/cm^3)**			
		10	*25*	*50*	*75*
Particle Diameter (µm)	*1*	0	559	553	541
	2.5	554	550	564	555
	5	550	560	557	553
	7.5	550	559	555	563
	10	557	557	556	550
	12.5	547	551	565	551
	15	542	549	551	552
	17.5	557	551	565	566

Table B3. 2D Laminar particle deposition at tracheal boundary for particle diameters and lower particle densities at an inhalation rate of 45 L/min.

Inhalation rate = 45 L/min		**Particle Density (g/cm^3)**			
		10	*25*	*50*	*75*
Particle Diameter (µm)	*1*	0	661	663	672
	2.5	666	671	669	666
	5	672	667	668	657
	7.5	666	665	679	656
	10	662	674	655	657
	12.5	666	663	651	673
	15	670	674	675	673

	17.5	657	661	676	687

Table B4. 2D Laminar particle deposition at tracheal boundary for particle diameters and lower particle densities at an inhalation rate of 60L/min

Inhalation rate = 60 L/min		**Particle Density (g/cm^3)**			
		10	*25*	*50*	*75*
Particle Diameter (µm)	*1*	0	767	765	756
	2.5	761	760	775	751
	5	749	766	753	763
	7.5	758	751	726	746
	10	761	726	779	740
	12.5	769	718	754	774
	15	767	769	761	767
	17.5	729	748	774	777

Table B5. 2D Laminar particle fraction deposition at tracheal boundary for particle diameters and lower particle densities at an inhalation rate of 15 L/min.

Inhalation rate = 15 L/min		**Particle Density (g/cm^3)**			
		10	*25*	*50*	*75*
Particle Diameter (µm)	*1*	0	.0544	.0545	.0541
	2.5	.0541	.0542	.0543	.0543
	5	.0543	.054	.0543	.0545
	7.5	.0544	.0548	.0542	.0549
	10	.0547	.0543	.0544	.0543
	12.5	.0544	.0547	.0546	.0543
	15	.0551	.0545	.0549	.0544
	17.5	.0549	.0544	.0545	.0547

Table B6. 2D Laminar particle fraction deposition at tracheal boundary for particle diameters and lower particle densities at an inhalation rate of 30 L/min.

Inhalation rate = 30	**Particle Density (g/cm^3)**

L/min		*10*	*25*	*50*	*75*
Particle Diameter (µm)	*1*	0	.0559	.0553	.0541
	2.5	.0554	.055	.0564	.0555
	5	.055	.056	.0557	.0553
	7.5	.055	.0559	.0555	.0563
	10	.0557	.0557	.0556	.055
	12.5	.0547	.0551	..0565	.0551
	15	.0542	.0549	.0551	.0552
	17.5	.0557	.0.551	.0565	.0566

Table B7. 2D Laminar particle fraction deposition at tracheal boundary for particle diameters and lower particle densities at an inhalation rate of 45 L/min.

Inhalation rate = 45 L/min		**Particle Density (g/cm^3)**			
		10	*25*	*50*	*75*
Particle Diameter (µm)	*1*	0	.0661	.0663	.0672
	2.5	.0666	.0671	.0669	.0666
	5	.0672	.0667	.0668	.0657
	7.5	.0666	.0665	.0679	.0656
	10	.0662	.0674	.0655	.0657
	12.5	.0666	.0663	.0651	.0673
	15	.0670	.0674	.0675	.0673
	17.5	.0657	.0661	.0676	.0687

Table B8. 2D Laminar particle fraction deposition at tracheal boundary for particle diameters and lower particle densities at an inhalation rate of 60 L/min.

Inhalation rate = 60 L/min		**Particle Density (g/cm^3)**			
		10	*25*	*50*	*75*
Particle Diameter (µm)	*1*	0	.0767	.0765	.0756
	2.5	.0761	.0760	.0775	.0751
	5	.0749	.0766	.0753	.0763
	7.5	.0758	.0751	.0726	.0746
	10	.0761	.0726	.0779	.0740
	12.5	.0769	.0718	.0754	.0774
	15	.0767	.0769	.0761	.0767
	17.5	.0729	.0748	.0774	.0777

Table B9. 2D Laminar particle fraction deposition at tracheal boundary for particle diameters and higher particle densities at an inhalation rate of 15 L/min.

Inhalation rate = 15 L/min		**Particle Density (g/cm^3)**				
		100	*200*	*400*	*600*	*800*
Particle	*1*	0.0541	0.0538	0.0541	0.0542	0.0542

Diameter (µm)	*2.5*	0.0544	0.0544	0.0544	0.0539	0.0538
	5	0.054	0.0539	0.0538	0.054	0.0541
	7.5	0.0546	0.0539	0.0545	0.0547	0.0535
	10	0.0539	0.0541	0.0544	0.0549	0.0553
	12.5	0.0543	0.055	0.0547	0.0542	0.0549

Table B10. 2D Laminar particle fraction deposition at tracheal boundary for particle diameters and higher particle densities at an inhalation rate of 30 L/min.

Inhalation rate = 30 L/min		**Particle Density (g/cm^3)**				
		100	*200*	*400*	*600*	*800*
Particle Diameter (µm)	*1*	0.0491	0.0485	0.0486	0.0483	0.0483
	2.5	0.0481	0.0491	0.0491	0.0506	0.0505
	5	0.0498	0.0508	0.0512	0.0512	0.0525
	7.5	0.0495	0.0507	0.0537	0.0574	0.0578
	10	0.0508	0.052	0.0573	0.0611	0.0597
	12.5	0.0516	0.0567	0.0602	0.0605	0.058

Table B11. 2D Laminar particle fraction deposition at tracheal boundary for particle diameters and higher particle densities at an inhalation rate of 45 L/min.

Inhalation rate = 45 L/min		**Particle Density (g/cm^3)**				
		100	*200*	*400*	*600*	*800*
Particle Diameter (µm)	*1*	0.0648	0.0641	0.0652	0.0651	0.064
	2.5	0.0639	0.0642	0.0656	0.0635	0.0612
	5	0.0649	0.0633	0.0641	0.0635	0.0631
	7.5	0.0626	0.0624	0.0637	0.0643	0.066
	10	0.063	0.0649	0.0653	0.0646	0.0677
	12.5	0.0647	0.0631	0.0657	0.0693	0.0692

Table B12. 2D Laminar particle fraction deposition at tracheal boundary for particle diameters and higher particle densities at an inhalation rate of 60 L/min.

Inhalation rate = 45 L/min		**Particle Density (g/cm^3)**				
		100	*200*	*400*	*600*	*800*
Particle Diameter (µm)	*1*	0.0828	0.0841	0.0834	0.0853	0.0852
	2.5	0.086	0.0842	0.0854	0.0864	0.0866
	5	0.0862	0.0849	0.0846	0.0855	0.0872
	7.5	0.0837	0.0875	0.0859	0.0859	0.0843
	10	0.0863	0.0871	0.0857	0.0828	0.0789
	12.5	0.0843	0.0856	0.0826	0.0787	0.0752

Table B13. Particle deposition fractions for the varying insertion angle at an inhalation rate of 15 L/min.

Inhalation rate = 15 L/min		Particle Density (g/cm^3)							
		10	25	50	75	100	200	400	600
Insertion Angle	-10	0.0547	0.0546	0.0546	0.0546	0.0547	0.0542	0.0542	0.0551
	-5	0.0546	0.0545	0.055	0.0544	0.0545	0.0549	0.0548	0.0557
	0	0.0546	0.0547	0.0549	0.0546	0.0546	0.0544	0.0543	0.0555
	5	0.0545	0.0546	0.0549	0.0547	0.0547	0.0543	0.0541	0.0548
	10	0.0545	0.0546	0.0549	0.0547	0.0547	0.0543	0.0541	0.0548

Table B14. Particle deposition fractions for the varying insertion angle at an inhalation rate of 30 L/min.

Inhalation rate = 30 L/min		Particle Density (g/cm^3)							
		10	25	50	75	100	200	400	600
Insertion Angle	-10	0.0531	0.0521	0.0501	0.052	0.052	0.0529	0.0574	0.0591
	-5	0.053	0.0514	0.0519	0.0527	0.053	0.0528	0.0567	0.0587
	0	0.0527	0.0515	0.05	0.0496	0.0517	0.0519	0.0568	0.0584
	5	0.0537	0.052	0.0494	0.0474	0.0489	0.0508	0.0571	0.0587
	10	0.053	0.0513	0.0535	0.0503	0.0506	0.0512	0.0656	0.059

Table B15. Particle deposition fractions for the varying insertion angle at an inhalation rate of 45 L/min.

Inhalation rate = 45 L/min		Particle Density (g/cm^3)							
		10	25	50	75	100	200	400	600
Insertion Angle	-10	0.0613	0.0604	0.0618	0.0629	0.0632	0.0654	0.0675	0.0654
	-5	0.0623	0.0617	0.0631	0.0621	0.0624	0.0659	0.0676	0.0667
	0	0.062	0.0624	0.0614	0.0624	0.0628	0.0644	0.0686	0.0673
	5	0.0605	0.0633	0.0621	0.0624	0.0614	0.064	0.0676	0.0667
	10	0.0629	0.0619	0.0613	0.062	0.0633	0.0657	0.0662	0.0665

Table B16. Particle deposition fractions for the varying insertion angle at an inhalation rate of 60 L/min.

Inhalation rate = 60 L/min		Particle Density (g/cm^3)							
		10	25	50	75	100	200	400	600
Insertion Angle	-10	0.0782	0.0781	0.0798	0.0791	0.0787	0.0783	0.083	0.0788
	-5	0.0792	0.0792	0.0794	0.0785	0.08	0.0792	0.0813	0.0791
	0	0.0785	0.074	0.0779	0.078	0.0798	0.0779	0.0821	0.0785
	5	0.0786	0.0795	0.078	0.0791	0.0793	0.0778	0.0816	0.0792
	10	0.0783	0.0796	0.0787	0.0778	0.0806	0.0782	0.0831	0.0785

2D Turbulent

Table B13. Particle deposition fractions for different particle densities and diameters at an inhalation rate of 30 L/min.

Inhalation rate = 30 L/min		**Particle Diameter (µm)**							
		1e-6	*2.5e-6*	*5e-6*	*7.5e-6*	*10e-6*	*12.5e-6*	*15e-6*	*17.5e-6*
Particle Density (g/cm^3)	*100*	.013	.008	.011	.013	.007	.01	.012	.015
	200	.009	0	.012	.009	.01	.014	.016	.013
	400	.014	.014	.01	.012	.014	.016	.015	.011
	600	.008	.012	.01	.01	.011	.008	.008	.001
	800	.015	.01	.011	.015	.015	.007	.005	.003

Table B14. Particle deposition fractions for different particle densities and diameters at an inhalation rate of 45 L/min.

Inhalation rate = 45 L/min		**Particle Diameter (µm)**							
		1e-6	*2.5e-6*	*5e-6*	*7.5e-6*	*10e-6*	*12.5e-6*	*15e-6*	*17.5e-6*
Particle Density (g/cm^3)	*100*	.013	.016	0	0	.011	.014	.013	.011
	200	.013	.01	.014	.013	.014	.007	.013	.013
	400	.01	0	.011	.011	.013	.015	.013	.008
	600	.01	.007	.014	.013	.015	.014	.012	.004
	800	.01	.02	.016	.016	.015	.005	.006	.001

Table B15. Particle deposition fractions for different particle densities and diameters at an inhalation rate of 60 L/min.

Inhalation rate = 60 L/min		**Particle Diameter (µm)**							
		1e-6	*2.5e-6*	*5e-6*	*7.5e-6*	*10e-6*	*12.5e-6*	*15e-6*	*17.5e-6*
Particle Density	*100*	.011	.012	.013	.013	.014	.013	.013	.011
	200	.013	.011	.013	.012	.013	.009	.015	.011
	400	.009	.009	.01	.014	0	.009	.009	.01

(g/cm^3)	*600*	.012	.01	.012	.009	.012	.01	.012	.009
	800	.002	.013	.013	.016	.002	.002	.013	.013

APPENDIX C: Software Implementation

C1.Solver

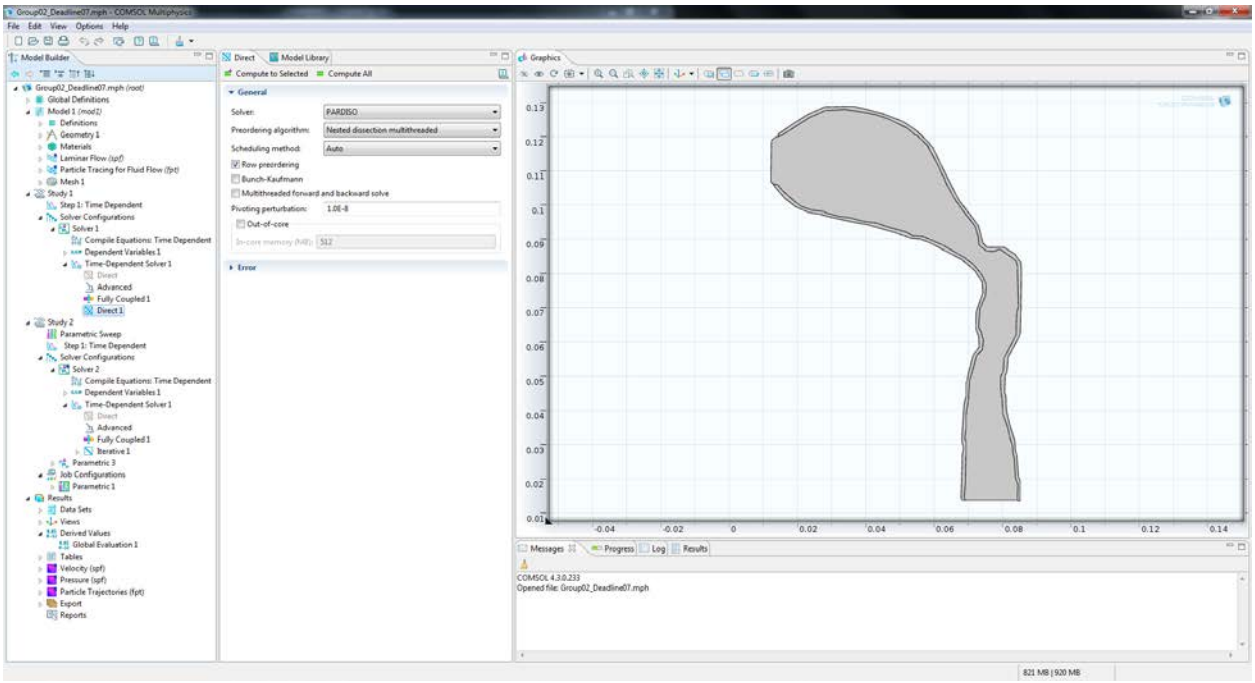

Fig C1. Direct solver for laminar flow in COMSOL.

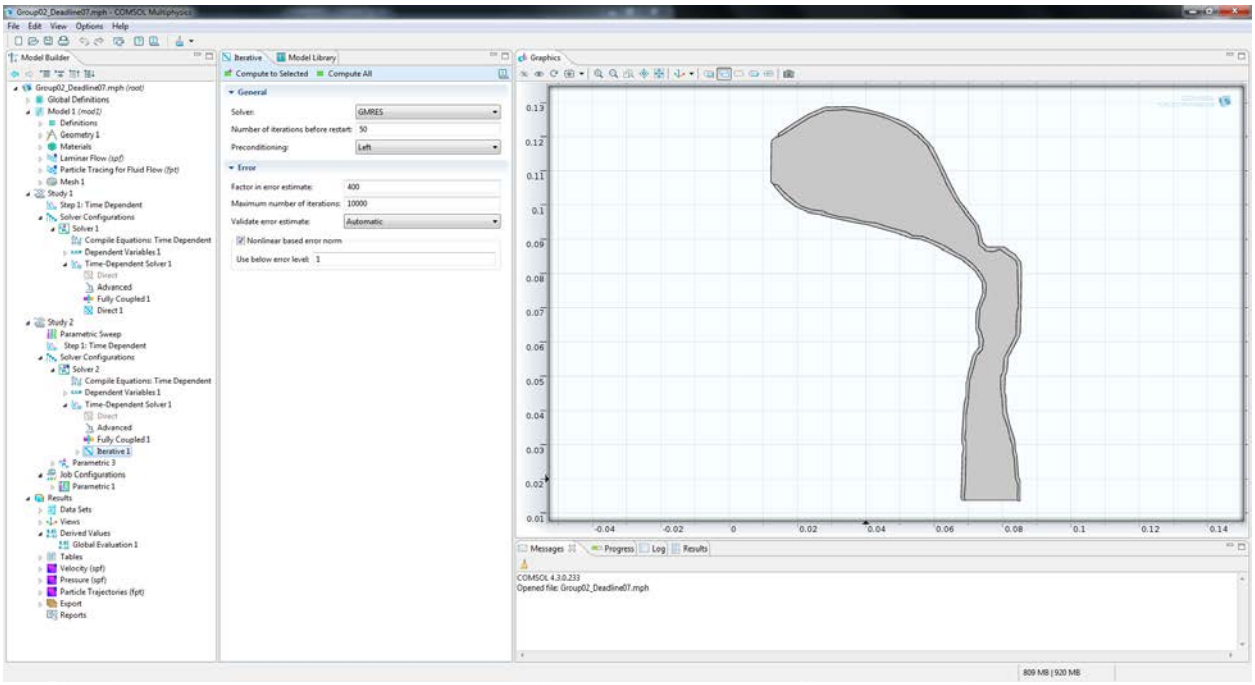

Fig C2. Iterative solver for particle tracing in COMSOL.

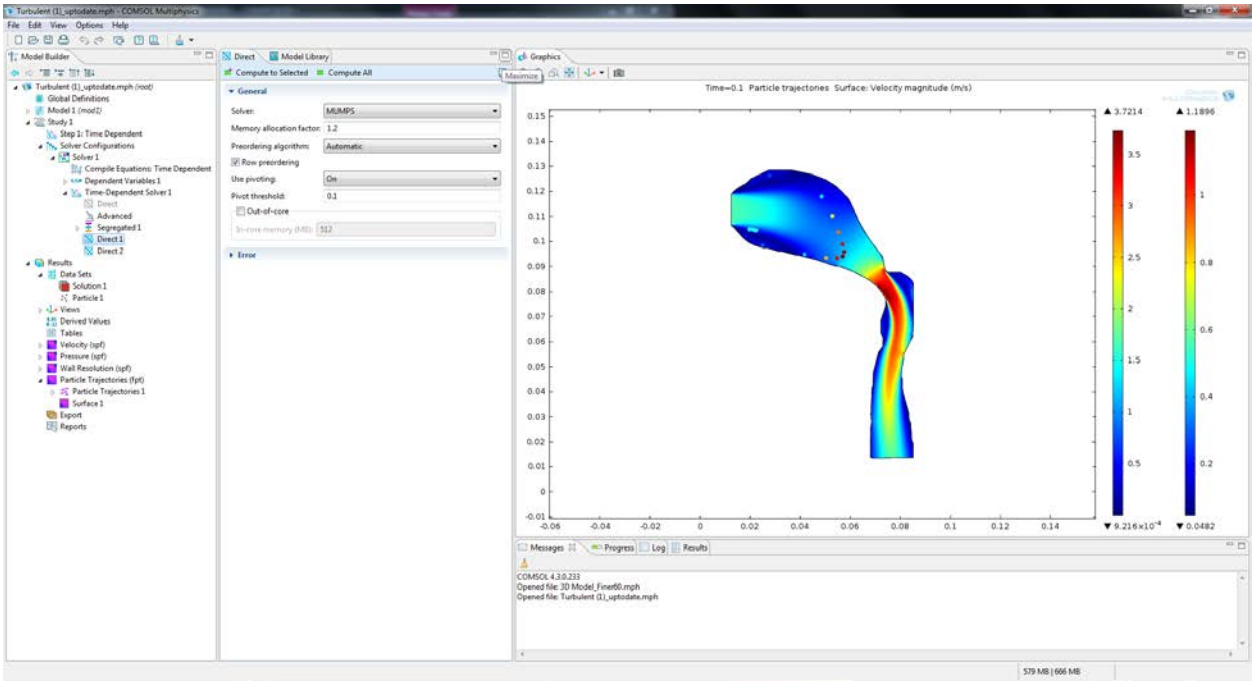

Fig C3. Direct solver for 2D turbulent flow in COMSOL.

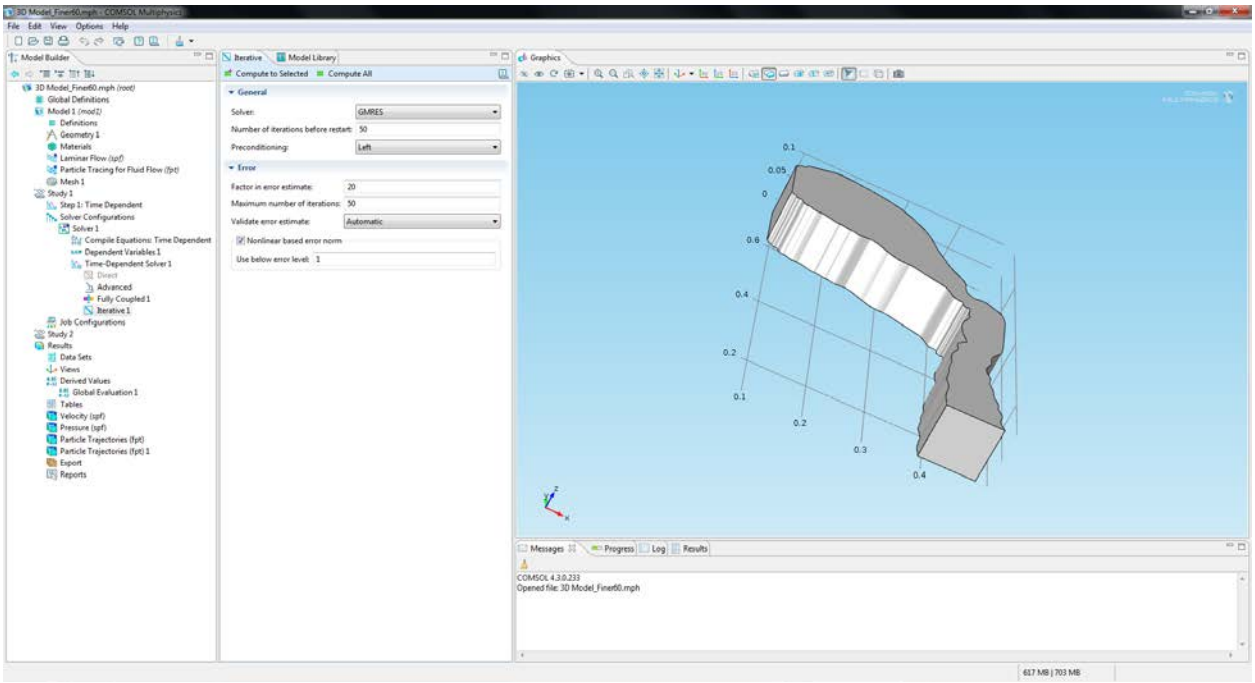

Fig C4. Iterative solver with maximum of 50 iterations for 3D laminar flow in COMSOL.

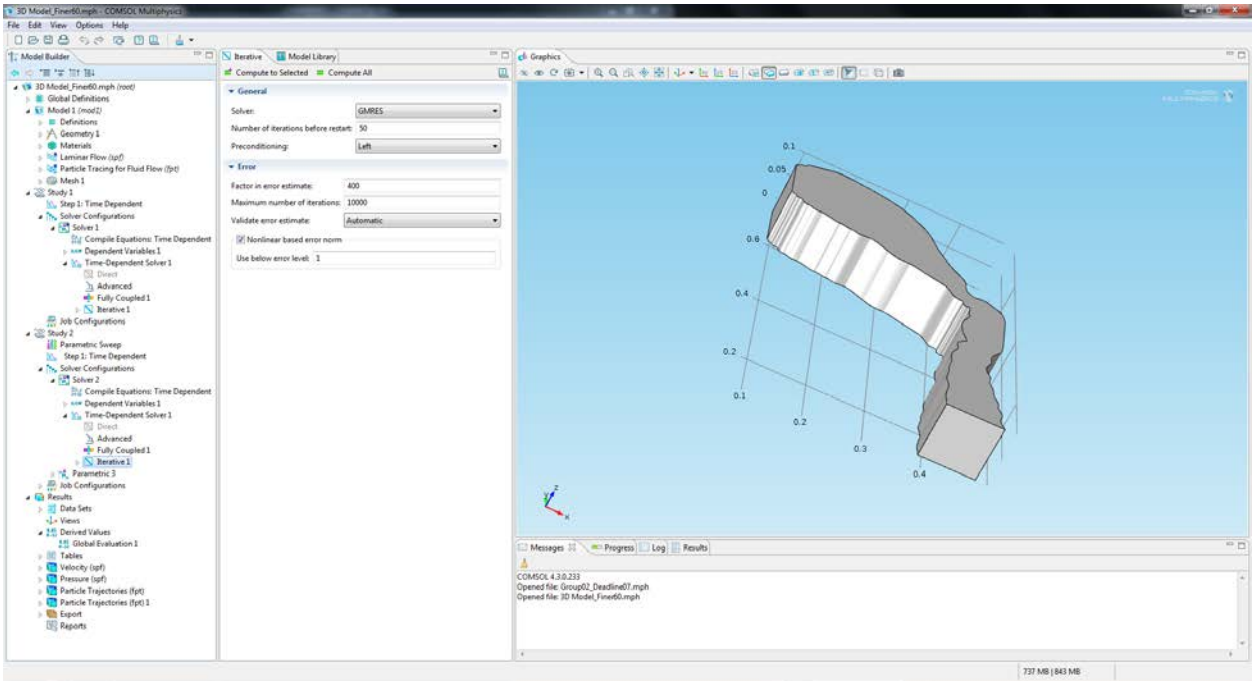

Fig C5. Iterative solver for particle tracing in 3D laminar flow in COMSOL.

C2. COMSOL Specifications

To run the 2D laminar flow model in COMSOL, the transient time stepping algorithm used was the “Laminar Flow” module. The time step used was 0.01 seconds and the relative tolerance was 0.8 (Fig C6A). Particle tracing was done in a separate solver using the “Particle Tracing for Fluid Flow” transient module with the same time step as that of the laminar flow module and a relative tolerance of 1.0E-5 (Fig C6C). The same specifications were used in the 3D laminar flow model, except that a relative tolerance of 0.01 was used for the “Laminar Flow” module (Fig C6B)

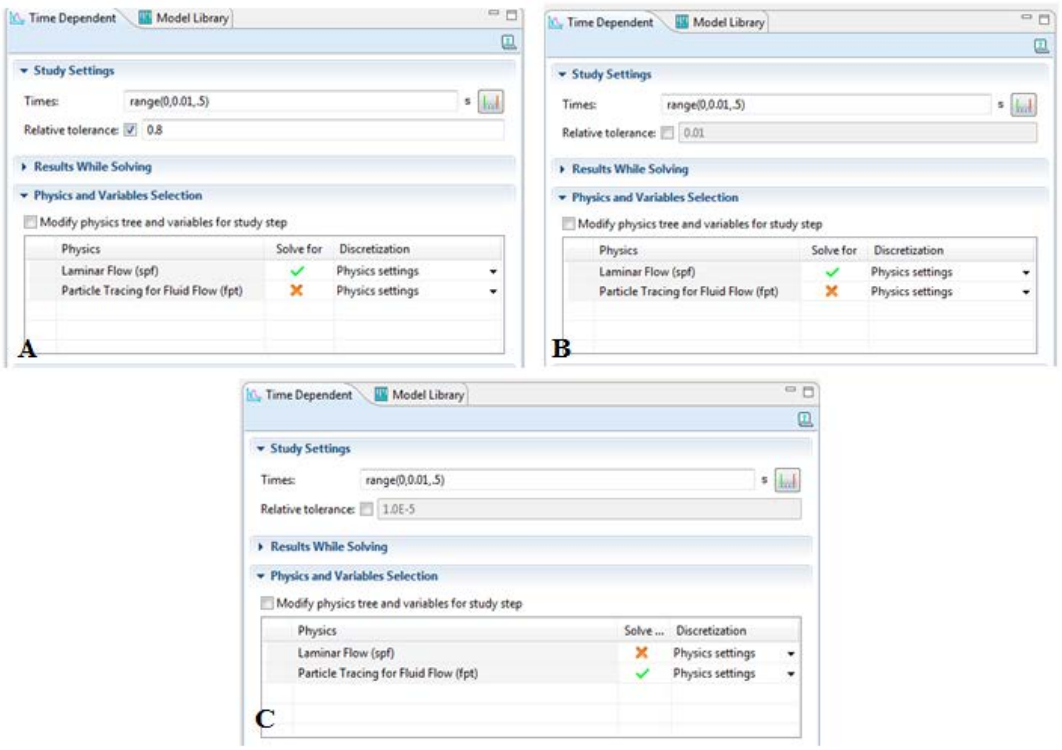

Figure C6: Specifcations for the "Laminar Flow" module in (A) for the 2D laminar model and in (B) for the 3D laminar model. The "ParticleTracing for Fluid Flow" module on in (C) was run in a separate solver for both models

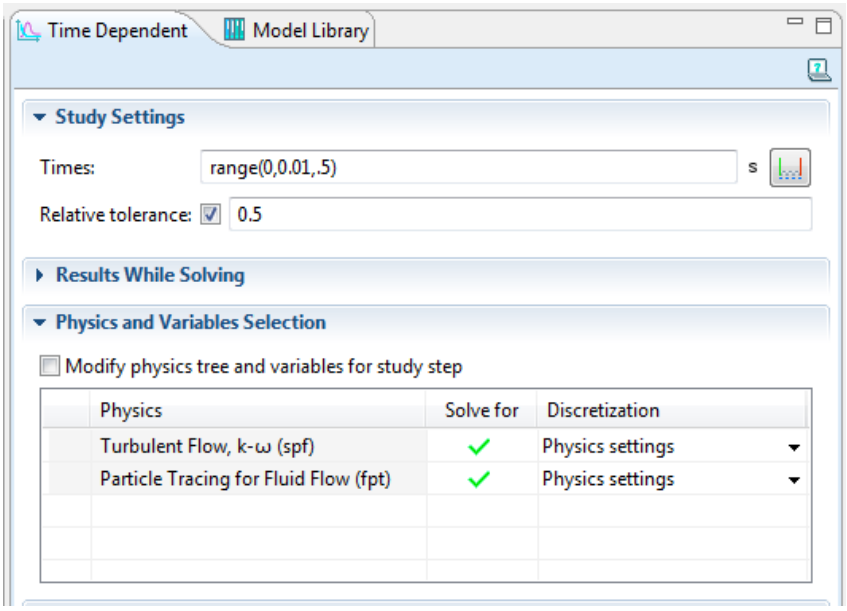

Fig C7: Specifications for the "Turbulent Flow, k-ω" and the "ParticleTracing for Fluid Flow" modules run in the same solver.

To run the 2D turbulent flow model in COMSOL, the transient time stepping algorithm used was the “Turbulent Flow, k-ω” module. The time step used was 0.01 seconds and the relative tolerance was 0.5 (Fig C7). Particle tracing was done in the same solver using the “Particle Tracing for Fluid Flow” transient module.

APPENDIX D: Additional visuals

D1.Turbulent Velocity Profile

The velocity profile was obtained for a cutline designated from point (0.0651, 0.0746) to point (0.0786, 0.0925), just as for the laminar model, by averaging the velocities over time for three different flow rates: 30 L/min and 60 L/min. The velocities were then normalized by dividing by the initial inlet velocity value. The time-averaged velocity profiles for both flow rates are nearly identical (Fig 3).

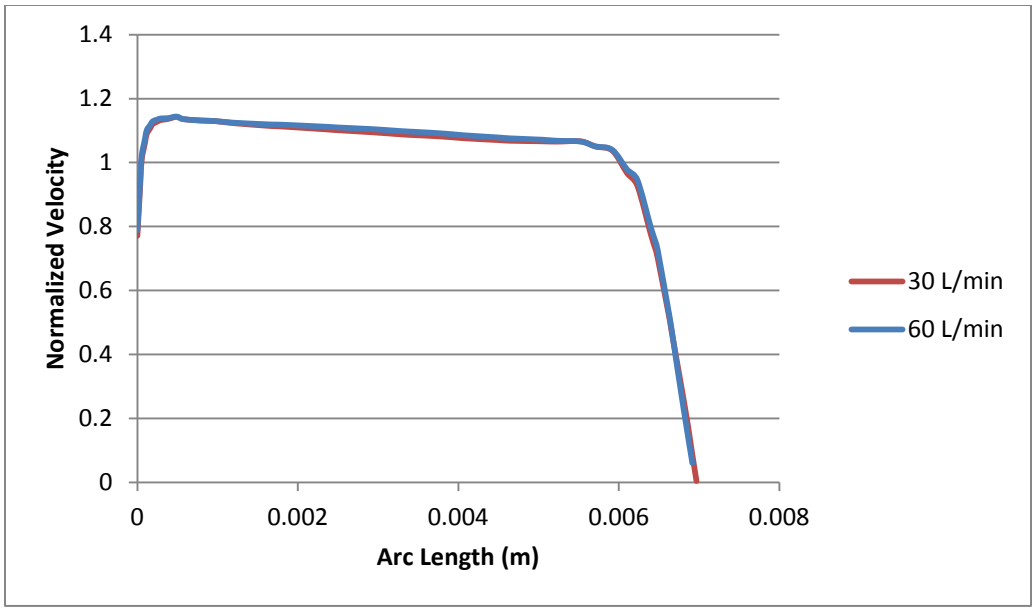

Figure D1: Velocity profiles averaged over time for 30 L/min and 60 L/min for cutline from point (0.0651, 0.0746) to point (0.0786, 0.0925).

APPENDIX E: References

[1] Yokoyama, H., Yamamura, Y., et. al. “Analysis of relationship between peak inspiratory flow rate and amount of drug delivered to lungs following inhalation of fluticasone propionate with Diskhaler.” *Biol Pharm Bull* (2007): 162-164

[2] Delvadia, Renish R., et al. "In Vitro Tests for Aerosol Deposition. III: Effect of Inhaler Insertion Angle on Aerosol Deposition." *Journal of Aerosol Medicine and Pulmonary Drug Delivery* (2012).

[3] Labiris, N., Dolovich, M. “Pulmonary drug delivery. Part I: Physiological factors affecting therapeutic effectiveness of aerosolized medications.” British Journal of Clinical Pharmacology (2003) 588-599

[4] Zanen, P. L. T. G., L. T. Go, and J. W. Lammers. "Optimal particle size for beta 2 agonist and anticholinergic aerosols in patients with severe airflow obstruction." *Thorax* 51.10 (1996): 977-980.

[5] Li, W. I., Perzl, M., Heyder, J., Langer, R., Brain, J. D., Englmeier, K. H., ... & Edwards, D. A. (1996). Aerodynamics and aerosol particle deaggregation phenomena in model oral-pharyngeal cavities. *Journal of aerosol science*, *27*(8), 1269-1286.

[6] Heenan, A. F., Matida, E., Pollard, A., & Finlay, W. H. (2003). Experimental measurements and computational modeling of the flow field in an idealized human oropharynx. *Experiments in Fluids*, *35*(1), 70-84.

[7] Jaroszczyk, T., & Wake, J. (1991). Critical Aerosol Velocity in Nonwoven Filtration. In *Proceeding of the 1991 TAPPI Nonwoven Conference* (pp. 125-135).

[8] Khassawneh, B. Y., Al-Ali, M. K., Alzoubi, K. H., Batarseh, M. Z., Al-Safi, S. A., Sharara, A. M., & Alnasr, H. M. (2008). Handling of inhaler devices in actual pulmonary practice: metered-dose inhaler versus dry powder inhalers.*Respiratory care*, *53*(3), 324-328.

[9] Tabak, L. A. (1995). In defense of the oral cavity: structure, biosynthesis, and function of salivary mucins. *Annual review of physiology*, *57*(1), 547-564.

[10] Jaroszczyk, T., & Wake, J. (1991). Critical Aerosol Velocity in Nonwoven Filtration. In *Proceeding of the 1991 TAPPI Nonwoven Conference* (pp. 125-135).

[11] Bronsky, E., Grossman, J., Henis, M., Gallo, P., Yegen, U., Cioppo, G., Kottakis, J., Mehra, S. “Inspiratory flow rates and volumes with the Aerolizer dry powder inhaler in asthmatic children and adults.” *Current Medical Research Opinion.* (2004) 20(2):131-7.

[12] Kleinstreuer, et. al. “Laminar-to-turbulent fluid-particle flows in a human airway model.” *International Journal of Multiphase Flow* (2003) pp. 271-289

[13] Heyder, J. (2004). Deposition of inhaled particles in the human respiratory tract and consequences for regional targeting in respiratory drug delivery.*Proceedings of the American Thoracic Society*, *1*(4), 315-320.

[14] Ghobrial, L. “Use of Inhaled Human Insulin in Paitents with Diabetes Mellitus.” *PharmacotherapyUpdate* (2007) X:1

[15] Rosenstock J, et. al. “Prandial inhaled insulin plus basal insulin glargine versus twice daily biaspart insulin for type 2 diabetes: a multicentre randomised trial” *Lancet* (2010); 375:2244

[16] Datta, Ashim K., and Vineet Rakesh. An Introduction to Modeling of Transport Processes: Applications to Biomedical Systems. Cambridge, UK: Cambridge UP, 2010. Print.

[17] Edwards, David A., et al. "Large porous particles for pulmonary drug delivery." *Science* 276.5320 (1997): 1868-1872